Using observed urban NO$_x$ sinks to constrain VOC reactivity and the ozone and radical budget in the Seoul Metropolitan Area

Benjamin A. Nault[1,2,*], Katherine R. Travis[3], James H. Crawford[3], Donald R. Blake[4], Pedro Campuzano-Jost[5], Ronald C. Cohen[6], Joshua P. DiGangi[3], Glenn S. Diskin[3], Samuel R. Hall[7], L. Gregory Huey[8], Jose L. Jimenez[5], Kyung-Eun Kim[9], Young Ro Lee[8,a], Isobel J. Simpson[4], Kirk Ullmann[7], Armin Wisthaler[10,11]

[1]CACC, Aerodyne Research, Inc., Billerica, MA, USA
[2]Department of Environmental Health and Engineering, Johns Hopkins University, Baltimore, MD, USA
[3]NASA Langley Research Center, Hampton, VA, USA
[4]Department of Chemistry, University of California, Irvine, CA, USA
[5]CIRES and Department of Chemistry, University of Colorado, Boulder, CO, USA
[6]Department of Chemistry, University of California, Berkeley, CA, USA
[7]Atmospheric Chemistry Observations & Modeling Laboratory, NCAR, Boulder, CO, USA
[8]School of Earth & Atmospheric Sciences, Georgia Institute of Technology, Atlanta, GA, USA
[9]School of Environmental Sciences and Environmental Engineering, Gwangju Institute of Science and Technology, Gwangju, South Korea
[10]University of Oslo, Oslo, Norway
[11]University of Innsbruck, Innsbruck, Austria

[a]Now at Division of Geological and Planetary Sciences, California Institute of Technology, Pasadena, CA, USA

[*]Corresponding author:
Email: bnault@aerodyne.com, bnault1@jh.edu

For ACP

Abstract

Ozone (O_3) is an important secondary pollutant that impacts air quality and human health. Eastern Asia has high regional O_3 background due to the numerous sources and increasing and rapid industrial growth, which impacts the Seoul Metropolitan Area (SMA). However, SMA has also been experiencing increasing O_3 driven by decreasing NO_x emissions, highlighting the role of local, in-situ O_3 production on SMA. Here, comprehensive gas-phase measurements collected on the NASA DC-8 during the NIER/NASA Korea United States-Air Quality (KORUS-AQ) study are used to constrain the instantaneous O_3 production rate over the SMA. The observed NO_x oxidized products support the importance of non-measured peroxy nitrates (PNs) in the O_3 chemistry in SMA, as they accounted for ~49% of the total PNs. Using the total measured PNs (ΣPNs) and alkyl and multifunctional nitrates (ΣANs), unmeasured volatile organic compound (VOC) reactivity (R(VOC)) is constrained and found to range from $1.4 - 2.1$ s^{-1}. Combining the observationally constrained R(VOC) with the other measurements on the DC-8, the instantaneous net O_3 production rate, which is as high as ~10 ppbv hr^{-1}, along with the important sinks of O_3 and radical chemistry, are constrained. This analysis shows that ΣPNs play an important role in both the sinks of O_3 and radical chemistry. Since ΣPNs are assumed to be in steady-state, the results here highlight the role ΣPNs play in urban environments in ~~reducing~~ altering net O_3 production, but ΣPNs can potentially lead to increased net O_3 production downwind due to their short lifetime (~1 hr). The results provide guidance for future measurements to identify the missing R(VOCs) and ΣPNs production.

50 **Short Summary**

51 Ozone (O_3) is a pollutant formed from the reactions of gases emitted from various sources. In

52 urban areas, the density of human activities can increase the O_3 formation rate ($P(O_3)$); thus, impact

53 air quality and health. Observations collected over Seoul, South Korea, are used to constrain $P(O_3)$.

54 A high local $P(O_3)$ was found; however, local $P(O_3)$ was partly reduced due to compounds typically

55 ignored. These observations also provide constraints for unmeasured compounds that will impact

56 $P(O_3)$.

1. Introduction

Representing global and urban tropospheric ozone (O_3) in chemical transport models (CTMs) is still challenging due to uncertainty in physical and chemical processes that control the O_3 budget (Archibald et al., 2020). One area of uncertainty is underestimated urban volatile organic compounds (VOCs) emissions (von Schneidemesser et al., 2023), which arise from a large number of sources, including some that are very hard to quantify (e.g., cooking and chemical products) (e.g., McDonald et al., 2018; Simpson et al., 2020). Intensive research is also ongoing as to why O_3 is increasing in recent years in urban areas, even with reductions in combustion emissions (Colombi et al., 2023; e.g., Lyu et al., 2017). This O_3 impacts the large populations in urban areas with harmful health effects, including premature mortality (e.g., Cohen et al., 2017).

Tropospheric O_3 production is driven by the catalytic cycling of nitrogen oxides (NO_x = $NO + NO_2$) fueled by the photoxidation of VOCs, both of which can come from anthropogenic emissions. The chemistry producing O_3 is described in R1 – R6 in Table 1. During daylight hours, VOCs are oxidized by OH (or undergo photolysis) to form an organic peroxy radical ($RO_2^{\cdot}$) in R1a (R1b). If the $RO_2^{\cdot}$ then proceeds through R2a, at least two O_3 molecules are produced. The first O_3 molecule is formed by the photolysis of NO_2 and the reaction of $O(^3P)$ with oxygen (R3 – R4). The second O_3 molecule is formed through the reaction of the alkoxy radical ($RO^{\cdot}$) with oxygen to form the hydroperoxyl radical (HO_2) (R5), which goes on to react with NO to produce NO_2 (R6) and the subsequent reactions described above (R3 – R4). However, some fraction of the time, depending on the number of carbons and functional group (e.g., Espada and Shepson, 2005; Perring et al., 2013; Yeh and Ziemann, 2014), alkyl or multifunctional nitrates (ANs ≡ $RONO_2$) are formed (R2b). The fraction of reactions to form ANs is described by the branching ratio, α. Reaction R2b has been shown to impact O_3 production, depending on the types of VOC emitted,

80   by reducing the fraction of NO_2 that photolyzes to form O_3 in source regions (R3 – R4) (Farmer et

81   al., 2011). As α is a function of the individual VOC's carbon backbone and functional group (e.g.,

82   Perring et al., 2013), any uncertainty related to primary VOC emissions and secondary chemistry

83   will directly impact the ability to describe urban O_3 production.

84   One important subclass of VOCs are aldehydes (RCHO), which can either be directly

85   emitted or produced via photooxidation of VOCs (de Gouw et al., 2018; Mellouki et al., 2015;

86   Wang et al., 2022; Yuan et al., 2012). The photooxidation of the aldehyde (R7) in the presence of

87   NO_x can either form acyl peroxy nitrates (R8, PNs = $R(O)O_2NO_2$) or an organic peroxy radical

88   ($RO_2^.$) (R9). The competition between R8 to form PNs versus R9 to form $RO_2^.$ depends on the

89   NO-to-NO_2 ratio (Nihill et al., 2021). Further, R8 is in thermodynamic equilibrium due to the weak

90   bond strength between the acyl peroxy radical ($R(O)O_2^.$) and NO_2. Thus, formation of PNs pose

91   only a temporary loss of NO_2. Finally, it has been observed that aldehydes with longer carbon

92   backbones (e.g., C8s and C9s) from various anthropogenic activities, such as cooking (Coggon et

93   al., 2024; Rao et al., 2010), may have mixing ratios as high as aldehydes typically quantified in

94   field experiments (acetaldehyde and propaldehyde). However, there is larger uncertainty

95   associated with these higher aldehydes in their fate to produce both PNs and ANs (e.g., Hurst

96   Bowman et al., 2003). Missing both these emissions and subsequent chemistry would impact

97   estimates of urban O_3 chemistry.

98   The fraction of $RO_2^.$ forming ANs in R2b and the fraction of $R(O)O_2^.$ forming PNs in R8

99   alter the instantaneous O_3 production (P(O_3)) by removing NO_2 and/or the radical species. This is

100   further shown in Figure S1, where an analytical equation to describe R1 – R6 (Farmer et al., 2011),

101   is used to explore how changes in the VOC reactivity (R(VOC)), radical production (P(HO_x)), and

102   ANs production and branching ratio, α (R2b), impact the instantaneous P(O_3) (see Sect. S1 for the

5

103   analytical equation and description). Any changes in $P(HO_x)$, $R(VOC)$, and/or α will impact both

104   the instantaneous $P(O_3)$ as well as the NO_x mixing ratio corresponding to the maximum $P(O_3)$. As

105   these parameters are generally interconnected, investigating all three is important to understand

106   the sources and control of instantaneous $P(O_3)$. Further, R7 – R9 are not included in this traditional

107   description of the analytical equation, as it is assumed PNs are in steady-state (Farmer et al., 2011).

108   Thus, if PNs are not in steady-state, their role in altering $P(O_3)$ may be underestimated.

109   Increasing surface O_3 is a concern throughout East Asia, including South Korea (Colombi

110   et al., 2023; Gaudel et al., 2018; Kim et al., 2021; Yeo and Kim, 2021). The emissions associated

111   with industry and other anthropogenic activities and the associated photochemistry have impacted

112   regional air quality, leading to high O_3 backgrounds that can impact a country's ability to achieve

113   reduced O_3 exposure for new air quality standards (e.g., Colombi et al., 2023). However, local

114   emissions and photochemistry still play an important role. For example, during the Korea-United

115   States Air Quality (KORUS-AQ) campaign, it was observed between morning and afternoon in

116   the Seoul Metropolitan Area (SMA), O_3 increased by ~20 parts per billion by volume (ppbv) over

117   a background concentration of over 75 ppbv (Crawford et al., 2021). Thus, an understanding of

118   the variables highlighted in Figure S1 are necessary to control both local and regional $P(O_3)$.

119   One tool typically used to understand the role of regional O_3 and transported O_3 on local

120   O_3 and impacts of local emission controls on O_3 are CTMs. As shown in Park et al. (2021), for the

121   SMA, CTMs typically underestimate the observed O_3 and formaldehyde. While the low O_3 could

122   be partially related to underestimated transport (e.g., Seo et al., 2018) or resolution of the CTM

123   (e.g., Jo et al., 2023; Park et al., 2021), the low bias also observed for modeled formaldehyde

124   indicates overall (a) too little VOCs and thus too low $R(VOC)$ (Brune et al., 2022; H. Kim et al.,

125   2022), (b) missing photochemical products from missing VOCs, including oxygenated VOCs

6

126 (OVOCs) that contribute to $P(HO_x)$ (Brune et al., 2022; H. Kim et al., 2022; Lee et al., 2022; Wang

127 et al., 2022), and (c) likely missing PNs and ANs from the underestimated VOCs related to the

128 underestimated R(VOC) (Lee et al., 2022; Park et al., 2021). Missing (a) – (c) will bias the

129 instantaneous $P(O_3)$ (Figure S1), impacting the ability to investigate what policies should be

130 implemented to reduce O_3.

131 To better understand what controls the instantaneous $P(O_3)$ over SMA, observations

132 collected on the NASA DC-8 during KORUS-AQ are used to constrain the three variables

133 highlighted in Figure S1—R(VOC), HO_x production and loss, and ANs and PNs production.

134 Observational constraints on these three parameters provide a means to investigate the

135 instantaneous $P(O_3)$ over SMA and the major classes of contributors to O_3 and HO_x production

136 and loss. These results are discussed and placed into the context of improving our knowledge about

137 O_3 production in an urban environment.

138

139 **2. Methods and Data Description**

140 **2.1 KORUS-AQ and DC-8 Descriptions**

141 The KORUS-AQ campaign was a multi-national project that was conducted in May – June,

142 2016, led by South Korea's National Institute of Environmental Research (NIER) and United

143 States National Aeronautics and Space Administration (NASA). The project was conducted in

144 South Korea and the surrounding seas with numerous airborne platforms, research vessels, and

145 ground sites (Crawford et al., 2021). The study here focuses on the observations collected on the

146 NASA DC-8.

147 The instrument payload, flights, and observations have been described in other studies

148 (Brune et al., 2022; Crawford et al., 2021; Lee et al., 2022; Schroeder et al., 2020). Briefly, the

7

149 DC-8 was stationed at Osan Air Force Base, Pyeongtaek, South Korea, which is approximately 60

150 km south of Seoul. A total of 20 research flights were conducted with the DC-8. Part of each

151 research flights included a stereo-route in the SMA in the morning (~09:00 local time), midday

152 (~12:00 local time), and afternoon (~15:00 local time), which included a missed approach over

153 Seoul Air Base (< 15 km from Seoul city center) and a fly-over of the Olympic Park and Taehwa

154 Forest Research sites (Figure 1). A total of 55 descents over Olympic Park and 53 spirals over

155 Taehwa Forest Research site were conducted (Crawford et al., 2021). Only observations from the

156 DC-8 after 11:00 local time are used here to ensure that the boundary layer has grown and

157 stabilized and to minimize any influence from residual layer mixing into the boundary layer and/or

158 titration of O_3 by NO (R10). We analyze data collected below 2 km and between 127.10 – 127.67°E

159 and 37.22 – 37.69°N to focus on the boundary layer in the SMA without influence from industrial

160 emissions along the western South Korean coast (Crawford et al., 2021).

161   During KORUS-AQ, four different meteorological periods, as described by Peterson et al.

162 (2019), impacted the region. These periods included a Dynamic period from 1 – 16 May, where

163 there were a series of frontal passages; a Stagnant period from 17 – 22 May, where it was dry,

164 clear, and stagnant; Transport/Haze period from 25 – 31 May, where long-range transport and hazy

165 conditions with high humidity and cloud cover prevailed; and, a Blocking period from 1 – 7 June,

166 where ~~blocking conditions minimized transport~~a high pressure ridge is located to an area north of

167 lower pressure, which can preclude significant changes in synoptic meteorology and results in

168 occasional stagnant conditions/minimal pollution transport (Peterson et al., 2019). However, as

169 discussed in Sect. 3.2, conditions did not impact the general trends and chemistry and thus the

170 whole campaign has been analyzed together.

171   The observations used for the analysis are shown in Table 2, along with the associated

172   references. The 1-min merged data from the DC-8 is used here (KORUS-AQ Science Team, 2023).

173   For data missing due to frequency of measurements (e.g., VOCs from WAS), data was filled in a

174   similar approach as Schroeder et al. (2020), in that VOCs with missing data were filled by the

175   linear relationship of that VOC with VOCs measured more frequently. This step was necessary for

176   the observations used in the diel steady-state calculations described in Sect. 2.2. Note, the TD-LIF

177   NO_2 (see Table 2) was used throughout this study and discussed in Sect. S2 and Figure S2 – S43

178   as it generally agreed better with steady-state calculated NO_2-to-NO ratios and steady-state NO_2

179   than the chemiluminescence NO_2. Further, though PBzN was measured by GT-CIMS (Table 2), it

180   is not compared with calculated PBzN from F0AM (Sect. 2.2) as it may be underestimated due to

181   possible inlet losses, as discussed in Zheng et al. (2011).

182

183   **2.2 F0AM Box Model Diel Steady-State Calculations for Missing Reactivity and**

184   **Peroxynitrate Budget Analysis**

185   We use the F0AM box model (Wolfe et al., 2016) with chemistry from the MCMv3.3.1

186   (Jenkin et al., 2015) to simulate production of PNs and formaldehyde using 1-min merged data, as

187   described in Sect. 2.1. As in Schroeder et al. (2020), we simulate each 1-min merged aircraft

188   observation in through the full diurnal solar cycle mode (i.e., diel steady-state) until the diurnal

189   cycle for each unconstrained species reaches convergence within 1%. These unconstrained species,

190   such as formaldehyde, NO_2, and OH, are then evaluated to ensure consistency between F0AM

191   model and aircraft observations. We constrain concentrations of NO, O_3, H_2O_2, HNO_3, CO, CH_4,

192   H_2, PAN, PPN, and all measured or estimated VOCs given in Table 2 and Table S1 to calculate

193   HO_2, all organic peroxy and acyl peroxy radicals, and unmeasured PNs. To calculate the PAN and

194   PNs budget, Wwe allow the model to freely calculate NO_2, formaldehyde, acetaldehyde, and all

195   PNs, including PAN and PPN, for when calculating the budget of PNs. However, for the acyl

196   peroxy radical mixing ratios to calculate O_x and HO_x budget (Sect. 2.3), PAN and PPN were

197   constrained by observations. We use a dilution constant of 12 hours, according to Brune et al.

198   (2022). Model evaluation is discussed in Sect. 3.4. The contribution of individual VOCs to PAN

199   was calculated by reducing precursor VOCs by 20% and multiplying the resulting impact on the

200   peroxy acetyl radical ($CH_3C(O)O_2$) by 5. Other acyl peroxy nitrates (higher PNs) are lumped into

201   categories based on their primary precursor species from Table S2, species currently typically

202   measured (e.g., PPN) or contributes a large fraction of the total higher PNs budget (greater than

203   >2%; e.g., PHAN and MPAN).

204   Note, the reason PAN and PPN were constrained were due to uncertainties in the thermal

205   lifetime, temperature history, and dilution rate used in F0AM, which had larger impacts on the

206    $CH_3C(O)O_2$ and PAN than on other unconstrained compounds (e.g., OH and formaldehyde and

207   not shown; Brune et al. (2022)).Part of this larger impact is due to $CH_3C(O)O_2$ being one of the

208   most abundant radicals and one of the final radical products in the oxidation of numerous

209   compounds (e.g., Jenkin et al., 2015). We do not expect these uncertainties to impact the higher

210   PNs as (a) there are less precursors to form them compared to PAN and (b) they are expected to

211   have higher thermal stability compared to PAN due to longer carbon backbone (Kabir et al., 2014).

212

213

214   **2.3 Calculation of Instantaneous Ozone and HO_x Production and Loss**

215   An experimental budget for the production and loss of O_x ($O_x = O_3 + NO_2$) and HO_x (HO_x

216    $= OH + HO_2 + RO_2 + R(O)O_2$) is described here. NO_2 and O_3 are combined to reduce any potential

217   impact from titration via O_3 reaction with NO (R10). The budget analysis includes field-measured

10

Formatted: Indent: First line: 0.5"

218 quantities (mixing ratios and photolysis rates, Table 2), results from F0AM (Sect. 2.2), estimated

219 missing R(VOC) (Sect. 3.2) and published kinetic rate constants (see Table 1 for references). The

220 rate of production or destruction is calculated with the following equations (Eq. 1 – 7) below. Note,

221 these equations differ from Schroeder et al. (2020) in that (a) ANs and PNs chemistry are explicitly

222 included and (b) the reaction of O_3 with alkenes is excluded as this reaction contributed a minor

223 loss to O_3 (< 1%).

224 $$P_{O_x} = \sum_i (1-\alpha_{ieff})k_{RO_{2,i}+NO}[RO_{2,i}][NO] + k_{HO_2+NO}[HO_2][NO] \tag{1}$$

225 $$L_{O_x} = k_{NO_2+OH}[NO_2][OH] + k_{O_3+OH}[O_3][OH] + f \times j_{O^1D}[O_3] +$$

226 $$k_{HO_2+O_3}[HO_2][O_3] + net(PNs) \tag{2}$$

227 $$net(PNs) = \beta k_{R(O)O_2+NO_2}[R(O)O_2][NO_2] - (1-\beta)k_{decomposition}[PNs] \tag{3}$$

228 $$\beta = \frac{k_{RC(O)O_2+NO_2}[NO_2]}{k_{RC(O)O_2+NO_2}[NO_2]+k_{RC(O)O_2+NO}[NO]} \tag{4}$$

229 $$P(HO_x) = 2f \times j_{O^1D}[O_3] + 2j_{H_2O_2}[H_2O_2] + 2j_{CH_2O \to H+HCO}[CH_2O] + 2j_{CHOCHO}[CHOCHO] +$$

230 $$2j_{CH_3OOH}[CH_3OOH] + 2j_{CH_3CHO}[CH_3CHO] + 2j_{CH_3C(O)CH_3}[CH_3C(O)CH_3] +$$

231 $$2j_{CH_3CH_2C(O)CH_3}[CH_3CH_2C(O)CH_2] \tag{5}$$

232 $$L(HO_x) = k_{NO_2+OH}[NO_2][OH] + \sum_i \alpha_{eff}k_{RO_{2,i}+NO}[RO_{2,i}][NO] +$$

233 $$2k_{HO_2+HO_2}[HO_2][HO_2] + 2k_{RO_2+RO_2}[RO_2][RO_2] + 2k_{HO_2+RO_2}[HO_2][RO_2] + net(PNs) \tag{6}$$

234 $$[RO_2] = \frac{\sum_i k_{OH+VOC,i}[VOC_i][OH]}{(1-\alpha_{eff})k_{RO_2+NO}[NO]+k_{RO_2+HO_2}[HO_2]} \tag{7}$$

235 Here, k is the rate constant for compound, i, with the associated compound listed, α_{eff} is the

236 effective branching ratio for R2a and R2b for the observations (Sect. 3.2), f is the fraction that O^1D

237 that reacts with water to form OH versus reacting with a third body molecule to form O^3P, β is the

238 fraction the $R(O)O_2$ that reacts with NO_2 versus NO, and j is the measured photolysis frequency

11

239 (Table 2). In Eq. 5, only directly values directly measured on the DC-8 during KORUS-AQ are

240 included. As discussed in Wang et al. (2022) and Sect. 4.3,, this is most likely an underestimations

241 of P(HO$_x$). Note, R(O)O$_2$ is not included in Eq. 7 as (a) it is assumed the initial production of

242 R(O)O$_2$ is captured with the reaction of OH with VOC and (b) R(O)O$_2$ accounts for a small

243 fraction of the total RO$_2$ (< 10%). Not including R(O)O$_2$ in Eq. 7 may lead to a small

244 underestimation of total RO$_2$. Finally, HO$_2$ calculated from F0AM, rather than aircraft

245 measurements (Crawford et al., 2021), is used in the equations to determine the O$_x$ and HO$_x$ budget

246 (see Sect. S3, Figure S6).

247

248 **3. Observational constraints on NO$_x$ organic oxidation chemistry**

249 In the Sect. 3.1, the detailed observations from the DC-8 during KORUS-AQ provided

250 measurements that allow us to test our understanding of NO$_x$ oxidation into total NO$_z$ (NO$_z$ =

251 higher NO$_x$ oxides, including ΣPNs, ΣANs, HNO$_3$ and particulate nitrate, pNO$_3$), which is needed

252 for the remainder of the analysis. Sect. 3.2 to 3.4 will focus on the organic NO$_z$ chemistry. This is

253 due to the chemistry and dynamics impacting the total inorganic nitrate chemistry that has been

254 discussed recently (Jordan et al., 2020; Travis et al., 2022).

255

256 **3.1 NO$_x$ and its oxidation products**

257 The average NO$_x$ mixing ratios observed by the NASA DC-8 in the SMA below 2 km after

258 11:00 local time is shown in Figure 1. As NO$_x$ is mainly emitted from anthropogenic activities,

259 such as combustion emissions, in an urban environment, the largest NO$_x$ mixing ratios are

260 observed between Olympic Park and the missed approach, as this area included downtown SMA.

261 The missed approach included low level sampling at a military airport, which may have

262   contributed to the NO_x mixing ratios along with the activities throughout the SMA. As the DC-8

263   flies from the missed approach toward Taehwa Research Site, the NO_x mixing ratios decreases.

264   The combination of reduced emissions, chemical reactions, and dilution and mixing reduces the

265   NO_x mixing ratios away from the city. An understanding of these processes is important for urban

266   $P(O_x)$.

267   On the DC-8, there were multiple measurements of various speciated and total family

268   contribution towards NO_z (Table 2). The comparison of the speciated and measured NO_z is

269   investigated in Figure 2 for observations over SMA. When only speciated PNs (GT) and ANs (CIT

270   + WAS) and gas-phase nitrate (HNO_3) are compared to the NO_z (NO_y (NCAR) – (NO (NCAR) +

271   NO_2 (TD-LIF)), only 46% of the NO_z can be explained. This is not completely unexpected, as

272   multiple studies have indicated that the speciated ANs measurements are typically lower than the

273   total ANs measurements (Fisher et al., 2016; Perring et al., 2010). Further, pNO_3 has been found

274   to be important for total nitrate budget in the SMA (e.g., Travis et al., 2022). Chemiluminescence

275   measurements of gas-phase NO_y have been found to efficiently measure pNO_3, depending on the

276   sensitivity to pNO_3 enhancements or exclusions (Bourgeois et al., 2022); thus, it is expected that

277   missing ANs and pNO_3 are necessary to close the NO_z budget. Adding the measured pNO_3 to the

278   speciated PNs (GT) and ANs (CIT + WAS) and gas-phase nitric acid, 81% of NO_z can be

279   explained. This barely overlaps the combined uncertainty of the measurements (~26%). Total PNs

280   and ANs, measured by TD-LIF, are needed to close of the total NO_z budget.

281   The breakdown of the NO_z budget over the SMA as the airmasses photochemically ages

282   (decreasing NO_x contribution to total NO_y) is shown in Figure 2b. During KORUS-AQ, ~56% of

283   NO_z was inorganic (gas- and particle-phase nitrate), ranging from 52% to 62%; the remaining NO_z

284   was organic (PNs and ANs). Approximately 74% of the total ANs were not speciated (range 73%

13

285   to 76%). Speciated PNs species, such as PAN (peroxy acetyl nitrate), account for a mean 51% of

286   the total PNs (range 47 to 59%), much lower than typically observed in prior studies (e.g.,

287   Wooldridge et al., 2010). In these prior studies, the speciated PN species (typically PAN + PPN

288   (peroxy propionyl nitrate)) accounted for 90 – 100% of the ΣPNs, except for some select cases

289   attributed to poor inlet design (Wooldridge et al., 2010). PAN accounted for the majority of the

290   speciated PNs, with the remaining speciated PNs (PPN + PBzN (peroxy benzoyl nitrate) + APAN

291   (peroxy acryloyl nitrate)) accounting for ~1%. However, during KORUS-AQ, Lee et al. (2022)

292   observed that PAN contributed only 60% of calculated total PNs in industrial plumes near the

293   SMA. Thus, the VOC emissions in and near SMA potentially lead to PNs typically not directly

294   measured; this is explored more in Sect. 3.4

295   As NO_x decreases from ~30 ppbv to 4 ppbv, the contribution of organic NO_z increases

296   (Figure 2b). At about 4 ppbv, the contribution of organic NO_z starts to decrease. Further, the

297   contribution of the different organic NO_z species changes. For example, from ~30 ppbv to 4 ppbv,

298   the un-speciated ΣPNs contributes the majority of the organic NO_z budget (~39%). Below ~4 ppbv,

299   the contribution of un-speciated ΣPNs decreases and the PAN contribution increases. The change

300   in contribution of PNs is due to changes in the PN precursors (e.g., combination short-lived

301   precursors oxidizing to $CH_3C(O)O_2^.$ and thermal decomposition of the higher PNs (higher PNs =

302   ΣPNs – PAN)). On the other hand, the contribution of un-speciated ΣANs remains relatively

303   constant with NO_x (~6% of total NO_z). However, the type of ANs is most likely changing with

304   NO_x due to the lifetime of the ANs precursors and/or the lifetime of ANs. Less is known about the

305   lifetime of ANs derived from anthropogenically emitted VOCs compared to those from biogenic

306   VOCs (González-Sánchez et al., 2023; Picquet-Varrault et al., 2020; Zare et al., 2018). On average

307   unknown ANs and PNs account for ~24% of the observed NO_z on average. The differences in the

14

308 binned mean value for each species is greater than the uncertainty associated with its measurements

309 (maximum uncertainty 30%) and greater than the standard error of the mean, indicating that all the

310 percent differences shown here are real.

311

312 **3.2 Meteorological impact on NO_x oxidation**

313 As discussed in Sect. 2.1 and various prior studies, four different meteorological conditions

314 impacted the observations during KORUS-AQ (Peterson et al., 2019). The impact of the

315 meteorological conditions on NO_x oxidation was investigated by plotting two metrics of NO_x

316 oxidation—O_x versus ΣANs and ΣPNs versus formaldehyde (Figure 3). The implications of both

317 plots are further discussed in Sect. 3.3 and 3.4, respectively. Briefly, O_x versus ΣANs and ΣPNs

318 versus formaldehyde are competitive products from the reaction of $RO_2^{\cdot}$ or $R(O)O_2^{\cdot}$ with NO_x

319 (R2a versus R2b or R8 versus R9). The different meteorological periods corresponded to

320 differences in temperatures and amount of photolysis due to cloud cover (Peterson et al., 2019).

321 Thus, these different periods may impact gas-phase chemistry and/or VOC emissions. However,

322 as demonstrated in Figure 3, there are minimal systematic differences in the trends observed for

323 the two NO_x oxidation products as there is no systematic shift in the trends or scatter observed in

324 Figure 3. This suggests that the data does not have to be separated by meteorological conditions.

325

326 **3.3 Production of ANs to constrain R(VOC)**

327 Observations of un-speciated ANs and PNs imply missing VOCs that impact O_3 chemistry.

328 The relationship of ANs to O_x can provide a method to investigate this source. This relationship

329 provides an estimate of the effective branching ratio, α, for the observed VOC mix (Perring et al.,

330 2013 and references therein). The value of this relationship stems from the reactions discussed

15

331 above (R1 – R6) in that upon the oxidation of VOCs, some fraction of the time, $RO_2^{\cdot}$ reacts with

332 NO to form an AN molecule and the remainder of the time the reaction goes to form O_3. This is

333 expressed with the following equations:

334 $$P_{\Sigma ANs} = \sum \alpha_i \, k_{OH+VOCi}[OH][VOC_i] \tag{8}$$

335 $$P(O_x) = \sum_i \gamma_i (1 - \alpha_i) \, k_{OH+VOC_i}[OH][VOC_i] \tag{9}$$

336 Here, α is the effective branching ratio in the reaction of $RO_2^{\cdot}$ with NO to form ANs versus RO

337 (R2), k is the OH rate constant with VOC, i, and γ is the number of O_3 molecules formed per

338 oxidation of VOC, i. The reactivity weighted γ is, calculated for the observed and F0AM calculated

339 compounds species from F0AM using the values from MCM with Eq. 10, where γ for each

340 compound is taken from MCM (Jenkin et al., 2015) and accounts for potential for difference

341 number of O_3 molecules produced per channel per oxidation (e.g., xylene produces two O_3

342 molecules 60% of the time and one O_3 molecule 40% of the time). All the terms were defined for

343 Eq. 8 – 9.

344 $$\gamma_{eff} = \frac{\sum_i \gamma_i k_{OH+VOC_i}[OH][VOC_i]}{\sum_i k_{OH+VOC_i}[OH][VOC_i]} \tag{10}$$

345 The reactivity weighted γ, is found to be, on average, 1.53, which is lower than the value of 2

346 typically assumed in prior studies (e.g., Perring et al., 2013). This lower reactivity weighted γ is

347 due to the role of CO ($\gamma = 1$) and CH_2O ($\gamma = 1$) to the total reactivity. After the boundary layer

348 height has stabilized (e.g., after 11:00 am LT used here) and is near enough (e.g., less than 1 day

349 aging) to the VOC source to ignore deposition and entrainment, Eq. 8 and 9 can be combined to

350 approximate the change in O_x per molecule ΣAN formed:

351 $$\frac{\Delta O_x}{\Delta \Sigma ANs} \approx \frac{P_{O_x}}{P_{\Sigma ANs}} \approx \frac{1.53(1-\alpha)}{\alpha} \tag{11}$$

352 For this equation to be valid, α needs to be relatively small ($\alpha \ll 1$), which is true for VOCs, as

353 maximum α for the conditions of KORUS-AQ is expected to be 0.35 (Orlando and Tyndall, 2012;

Formatted: Font: Times New Roman, Not Italic

Formatted: Font: Times New Roman, Not Italic

Formatted: Font: Times New Roman, Not Italic

Formatted: Font: Times New Roman, Not Italic

Formatted: Font: Times New Roman, Not Italic

Formatted: Font: Times New Roman, Not Italic

Formatted: Font: Times New Roman, Not Italic

Formatted: Font: Times New Roman, Not Italic

354 Perring et al., 2013; Yeh and Ziemann, 2014). Note, though Eq. 1~~0~~1 can be used at short

355 photochemical ages due to minimal impact from physical loss processes, chemical loss processes

356 may impact the assumptions in Eq. 1~~0~~1 and are discussed in more detail below.

357   Over the SMA during KORUS-AQ, the slope between O_x and ΣANs was observed to be

358 40.5 ± 1.8 (Figure 3a), with an $R^2 = 0.60$. Using Eq. 1~~0~~1, this translates to an effective branching

359 ratio (α_{eff}), of 0.036. For other urban locations around the world, this slope has ranged from 13 –

360 47 (Farmer et al., 2011; Kenagy et al., 2020; Perring et al., 2010; Rosen et al., 2004), leading to an

361 effective α between 0.04 and 0.15, assuming a γ of 2 instead of the calculated γ used here. Thus,

362 the α_{eff} observed over SMA during KORUS-AQ is similar to other urban locations (Houston =

363 0.05 (Rosen et al., 2004) and South Korea = 0.05 (Kenagy et al., 2021)) but much lower than

364 observed for Mexico City = 0.07 – 0.12 (Farmer et al., 2011; Perring et al., 2010) and Denver =

365 0.16 (Kenagy et al., 2020). This suggests that VOCs with low α dominate the total R(VOC) and

366 production of ANs in SMA. The VOCs in SMA that dominate R(VOCs), including OVOCs,

367 alkenes, and aromatics (Schroeder et al., 2020; Simpson et al., 2020), generally have lower α

368 (Orlando and Tyndall, 2012; Perring et al., 2013 and references therein).

369   We use the observed VOCs (Table 2) and estimated secondary products from F0AM to

370 calculate α_{eff} from this mixture to compare to the calculated α_{eff} of 0.036 derived from the slope of

371 O_x versus ΣANs in Figure 3a, as shown in Figure 4. To derive α_{eff}, Eq. 12 was used, where all the

372 terms are the same as Eq. 8 – 9.

373 $$\alpha_{eff} = \frac{\sum_i \alpha_i k_{OH+VOC_i}[\text{OH}][\text{VOC}_i]}{\sum_i \gamma_i k_{OH+VOC_i}[\text{OH}][\text{VOC}_i]} \qquad (12)$$

374 The R(VOC) calculated from the observed VOCs and from the intermediates produced by the

375 F0AM model, described in Sect. 2.2, are shown in Figure 4a, and the reactivity weighted α for the

376 observations is shown in Figure 4b. As has been observed in other urban environments (e.g.,

17

377 Hansen et al., 2021; Whalley et al., 2016; Whalley et al., 2021; Yang et al., 2022), measured

378 OVOCs contribute the most to the calculated R(VOC) for all NO_x mixing ratios (32 – 48%). The

379 unmeasured OVOCs (F0AM species) contributed 17 – 28% of the calculated reactivity. The F0AM

380 species reactivity ranged from 0.45 – 1.78 s^{-1}, which is a similar increase in total OH reactivity

381 observed by Brune et al. (2022) over South Korea. At higher NO_x mixing ratios, primary, more

382 reactive VOCs (e.g., alkanes, alkenes, aromatics) contribute an important fraction (> 25%) of the

383 R(VOC). As there are interferences in the total OH reactivity measurement at high NO_x (Brune et

384 al., 2022), we are unable to determine the extent to which the observed and modeled reactivity

385 captures total OH reactivity in the SMA above a NO_x value of approximately 4 ppbv. At lower

386 NO_x mixing ratios, ~33% of the R(VOC) is missing (calculated R(VOC), including F0AM species,

387 ~3.0 s^{-1} and measured R(VOC) from Penn State—see Table 2—is 4.5 s^{-1}).

388   Numerous other urban studies have observed unmeasured OH reactivity, which is assumed

389 to be unmeasured R(VOC), as the inorganic OH reactivity is typically well covered by

390 measurements. Here, we are defining unmeasured R(VOC) as the reactivity not represented by

391 measurements on the DC-8 or by F0AM predicted species and reactivity. This unmeasured

392 R(VOC) has ranged from ~3 s^{-1} to ~10 s^{-1} (e.g., Brune et al., 2022; Hansen et al., 2021; Kim et al.,

393 2016; Ma et al., 2022; Tan et al., 2019; Whalley et al., 2016; Whalley et al., 2021). Over the SMA,

394 the difference between measured and calculated R(VOC) was ~1.5 s^{-1} at low NO_x and unknown at

395 high NO_x mixing ratios. The lower difference may be related to the comparison occurring for

396 observations at low NO_x, when the very reactive material has either reacted into compounds

397 measured on the DC-8 (e.g., formaldehyde, acetaldehyde, etc.), diluted to low enough

398 concentrations to be negligible for R(VOC), or undergone deposition or partitioning to the particle-

399 phase.

18

400 At higher NO$_x$ mixing ratios, which is more representative of fresh emissions, these more

401 reactive compounds typically not measured are expected to lead to a higher difference between the

402 calculated and observed R(VOC). Prior studies with more comprehensive measurements found

403 these more reactive compounds and their secondary products contributed an important fraction

404 towards the R(VOC) (e.g., Whalley et al., 2016). Thus, to determine if these unmeasured VOCs

405 potentially contribute to the R(VOC), and thus P(O$_x$), in SMA, another means to constrain their

406 contributions is necessary. One potential means to constrain the total R(VOC) is by using the

407 observed ΣANs and O$_x$ and assuming the observations are from the instantaneous production of

408 both species (e.g., the assumption used for Figure 3a).

409 To estimate the unmeasured R(VOC), Eq. 13θ is used without cancelling out terms and

410 expanded into the measured and unmeasured R(VOC) and α:

411 $$\frac{\Delta O_x}{\Delta \sum ANs} = \frac{\gamma RVOC_m[\text{OH}] + \gamma RVOC_u[\text{OH}] - \gamma \alpha_m RVOC_m[\text{OH}] - \gamma \alpha_u RVOC_u[\text{OH}]}{\alpha_m RVOC_m[\text{OH}] + \alpha_u RVOC_u[\text{OH}]}$$ (13$\mathbf{1}$)

412 Here, $\frac{\Delta O_x}{\Delta \sum ANs}$ is the slope from Figure 3a, γ is the number of O$_3$ molecules formed per oxidation of

413 VOC, which is 1.53 for this study, R(VOC) is the VOC reactivity, which is its OH oxidation rate

414 constant and its concentration (k×[VOC]) in units s^{-1}, α is the branching ratio for R2 (Table 1), and

415 *m* and *u* correspond to "measured" (measured VOCs on DC-8 along with secondary species

416 predicted by F0AM) and "unmeasured" (unmeasured VOCs that are not represented by DC-8

417 observations and not predicted by F0AM) RVOC and α. The rate constants for the measured VOCs

418 are listed in Table 1, the reactivity for F0AM is taken directly from F0AM, and α is either from

419 MCM (Jenkin et al., 2015) or Perring et al. (2013) for observations or assumed to be 0.05 for

420 F0AM secondary products. The equation is rearranged and solved for *RVOC$_u$*, using different

421 values of *α$_u$* (e.g., 0.00 – 0.30, values typical α).

422   As discussed in Sect. S3 in the Supp. Information, there are numerous assumptions and

423   potential sources of uncertainty in the simplified version of Eq. 13~~1~~. A thorough analysis and

424   discussion of these assumptions are discussed in Sect. S3. The potentially most important

425   assumption is that chemical loss is negligible in solving Eq. 13~~1~~. However, due to the expected

426   relatively short lifetime of $\sum$ANs, the chemical loss of both O_x and ANs nearly cancel each other,

427   leading to similar results in considering or neglecting these loss terms in Eq. 13~~1~~. Further, as $\sum$ANs

428   chemical loss has uncertainty, especially for ANs produced from anthropogenic VOC oxidation,

429   the use of Eq. 13~~1~~ reduces some of these uncertainties in comparison to Eq. S9. Thus, for the

430   remainer of the paper, the values calculated from Eq. 13~~1~~ will be used. Another limitation in this

431   study is assuming a constant α and γ across all NO_x mixing ratios to estimate the unmeasured

432   R(VOC). At higher NO_x mixing ratios, where the VOC mixing ratios would be highest due to

433   being closer to emissions, it would be expected that both α and γ would change. However, the

434   direction that these values would change is uncertain as both α and γ depend on the structure of

435   the VOC, which is currently unknown.

436   For the range of missing α assumed, an $\alpha = 0.10$ for the unmeasured R(VOC) provides the

437   best agreement with the observed R(VOC) ("From PSU" is the Penn State OH Reactivity with

438   inorganic reactivity subtracted out) for all observations where $NO_x < 4$ ppbv. Further, it is found

439   that α ranging from $0.075 - 0.125$ encompasses the associated uncertainty with the observed

440   R(VOC) (± 0.64 s^{-1} (Brune et al., 2019)). This leads to an average unmeasured R(VOC) of $1.7^{+1.1}_{-0.4}$.

441   The associated total missing R(VOC) for the assumed α of 0.10 ranges from 1.5~~4~~ to 2.8~~1~~

442   s^{-1} (Figure 4a upper panel). Assuming typical rate constants for emitted VOCs, assuming it is

443   comparable to semi- and intermediate-VOCs, and their associated secondary products ($\sim 1 - 4 \times 10^{-}$

444   ^{11} cm^3 molec.$^{-1}$ s^{-1} (Ma et al., 2017; Zhao et al., 2014)), the total missing reactivity would be

20

445 equivalent to ~1 – 8 ppbv. Zhao et al. (2014) observed ~12 μg m^{-3} of semi- and intermediate-VOCs

446 near Los Angeles, CA, during the CalNex study. Depending on the molecular weight assumed,

447 this translates to ~1 to 2 ppbv. Nault et al. (2018) found that ~5 – 8 ppbv of VOCs were needed to

448 explain the observed secondary organic aerosol production over the SMA, depending on the

449 molecular weight assumed for the VOC. Further, Kenagy et al. (2021) also found that known

450 chemistry could only account for ~33% of the observed ANs and missing sources of lower

451 volatility VOCs to produce anthropogenically-derived ANs were necessary. Finally, Whalley et

452 al. (2016) found that addition of unassigned VOCs and their associated oxidation products led to

453 a reactivity of ~1.6 s^{-1}, leading to ~1 – 6 ppbv missing R(VOC). Thus, the reactivity and equivalent

454 mixing ratios estimated here appear plausible and warrant future measurements to understand this

455 unmeasured reactivity sources.

456   One important aspect of this unmeasured R(VOC) is that it should not be considered one

457 or a couple of VOCs emitted and contributing 1 – 8 ppbv of VOC in the atmosphere. Instead, it

458 will be the emitted VOCs and its oxidation products summed together to form the 1 – 8 ppbv of

459 unmeasured VOCs in the atmosphere.

460   One possible group of missing VOCs ~~is~~ are long-chain aldehydes from cooking and

461 vegetative emissions, including nonanal~~, which is associated with cooking emissions~~ (Hurst

462 Bowman et al., 2003; Rao et al., 2010; Sai et al., 2012; Schauer et al., 2002)~~ and vegetative~~

463 ~~emissions~~. Kim et al. (2018) observed cooking organic aerosols at a ground site in SMA, indicating

464 that there should be associated gas-phase emissions from cooking. Higher carbon aldehydes (or

465 cycloalkanes)~~Nonanal~~ ~~has~~ have been recently ~~been~~ suggested to be a potential interference

466 compound with isoprene measurements on a PTR-MS (Coggon et al., 2024; Wargocki et al., 2023).

467 Comparisons of isoprene measured by the PTR-MS and WAS during KORUS-AQ (Figure S7~~5~~)

468   shows at increasing NO_x mixing ratios (closer to emission sources), the difference between the

469   PTR-MS and WAS isoprene mixing ratios increases. This suggests that there are potential

470   unmeasured OVOCs and/or other C_5H_8 alkenes at high NO_x ratios that cannot be easily determined

471   by the difference between the PTR-MS and WAS. Continuing to use nonanal as a surrogate for

472   this unmeasured OVOC, nonanal has a rate constant consistent with the values used above for the

473   missing R(VOC) (3.6×10^{-11} cm^3 molec.$^{-1}$ s^{-1} (Hurst Bowman et al., 2003)). Further, nonanal has

474   an estimated high α of ~0.2 (Hurst Bowman et al., 2003). As typical nonanal mixing ratios have

475   been observed or estimated to be < 500 pptv, this suggests that nonanal or similar OVOCs may

476   contribute to some of the missing reactivity (< 0.45 s^{-1}). Finally, nonanal and other long-chain

477   aldehydes may be an important higher PNs precursor (see Sect. 3.4 for more discussion about un-

478   speciated higher PNs).

479   OVOC emissions from multiple sources, including solvent evaporation and other non-

480   transportation emissions, are generally considered to be an important fraction of R(VOC) for urban

481   emissions but may not be measurable by PTR or GC, such as glycols (de Gouw et al., 2018;

482   Gkatzelis et al., 2021; McDonald et al., 2018; Ma et al., 2022; Simpson et al., 2020; Wang et al.,

483   2022; Yang et al., 2022). However, the α for OVOC is potentially smaller than alkanes, though it

484   is highly unconstrained (Orlando and Tyndall, 2012). Note, higher OVOCs have been understudied

485   and thus may have higher α (e.g., nonanal). Thus, if the missing reactivity is mainly OVOCs and

486   it is assumed their α is low, compounds with $\alpha > 0.15$ will be needed for the budget closure shown

487   here. Likely compounds with high α include alkanes, cycloalkenes/alkenes, and aromatics, though

488   the latter is also highly uncertain. Alkanes have typically been a small source for the R(VOC) in

489   urban environments (e.g., McDonald et al., 2018; Simpson et al., 2020; Whalley et al., 2016).

490   Though aromatics contribute a significant fraction of R(VOC) in different Asian urban

22

491 environments (Brune et al., 2022; Schroeder et al., 2020; Simpson et al., 2020; Whalley et al.,

492 2021), the majority of the aromatic R(VOC) is considered to be measured by WAS over SMA

493 during KORUS-AQ (e.g., measured aromatics account for ~81% of aromatic reactivity in

494 McDonald et al. (2018) and 98% of aromatic reactivity in Whalley et al. (2016), where both studies

495 had more complete VOC measurements). Finally, the cycloalkenes/alkenes originate from

496 numerous anthropogenic sources (e.g., McDonald et al., 2018; Simpson et al., 2020). One subclass

497 of cycloalkenes includes monoterpenes. Similar to the comparison of isoprene between PTR-MS

498 and WAS, the difference in monoterpenes between these two measurements increases with

499 increasing NO_x (Figure S86). As the interfering compound(s) measured by the PTR-MS and

500 whether they are oxygenated or not is not known, only the WAS monoterpenes are used in this

501 analysis of calculating R(VOC). Assuming the limonene rate constant, the difference between the

502 PTR-MS and WAS monoterpenes raises the terpene reactivity by $0.05 – 0.30$ s^{-1}. Though this does

503 not include any associated photochemical products from the oxidation of monoterpenes and can

504 improve the closure, it does not explain the total missing reactivity ($1.4 – 2.1$ s^{-1}). Thus, the missing

505 R(VOC) is most likely a combination of OVOCs and cycloalkenes/alkenes.

506

507 **3.4 Sources of PNs over SMA**

508   As shown in Figure 2, ΣPNs account for a larger fraction of the total NO_z budget than

509 ΣANs. ΣPNs are known to be a temporary sink of NO_x and radicals ($R(O)O_2$) due to their short

510 thermal lifetime (~1 hr). Thus, the NO_x emitted in SMA is being transported regionally, impacting

511 the $P(O_x)$.

512   In Figure 3b, ΣPNs shows some correlation with formaldehyde. Both are secondary

513 products from the photooxidation of VOCs and have short lifetimes, leading to the correlation.

23

514 However, above 4 ppbv formaldehyde, the correlation shifts as ΣPNs increases more rapidly than

515 formaldehyde. As shown in Figure S9~~7~~, this change in the relationship between ΣPNs versus

516 formaldehyde is due to changes in the competition in the reaction of the acyl peroxy radical

517 $(R(O)O_2^{\cdot})$ between NO_2 and NO. At low NO-to-NO_2 ratios, R8 is more favorable, as the $R(O)O_2^{\cdot}$

518 is more likely to react with NO_2 compared with NO, leading to more efficient production over

519 formaldehyde. As the NO-to-NO_2 ratios increase (NO becomes comparable to NO_2, leading to

520 more equal probability in $R(O)O_2^{\cdot}$, reacting to NO and NO_2, leading to production of alkoxy

521 radicals that can form formaldehyde), R9 becomes more dominant, leading to less production of

522 PNs. ~~leading to more efficient production of PNs over formaldehyde. As NO to NO₂ ratios~~

523 ~~increase (NO becomes comparable to NO₂), R9 becomes more dominant, leading to less~~

524 ~~production of PNs.~~

525   To further explore the sources of both PAN and the higher ΣPNs, the F0AM model (Wolfe

526 et al., 2016) was used to predict both unmeasured ΣPNs, constrained by the observed VOCs

527 precursors, PAN, and PPN (Table 2) and budget of all ΣPNs, where PAN and PPN were not

528 constrained. F0AM shows minimal bias in the predicted formaldehyde, NO_2, and OH (Figure

529 S10~~8~~) when PAN and PPN were constrained. As discussed in Sect. 3.3, though, there is missing

530 R(VOC) of $1.7^{+1.1}_{-0.4}s^{-1}$. A sensitivity analysis in adding this missing reactivity to F0AM on

531 predicted OH and formaldehyde was conducted (Sect. S4 and Figure S11~~9~~ – S12~~0~~). Both OH and

532 formaldehyde are found to be buffered with the addition of this low amount of R(VOC). Thus,

533 though there is good agreement in these intermediate products between observation and F0AM,

534 this analysis for the sources of PAN and higher ΣPNs is expected to be a lower limit. This missing

535 R(VOC) is further observed in the F0AM-predicted higher PNs (ΣPNs without PAN, or ΣPNs-

536 PAN for short) versus formaldehyde, as a general underestimation in the total higher PNs

24

537 compared to observations is observed (Figure 5a). ~~PAN was excluded as F0AM overestimated the~~

538 ~~mixing ratios of PAN by approximately a factor of 2 (Figure S8e). Note, F0AM also overpredicted~~

539 ~~the PPN mixing ratios, but to a lesser extent than PAN (~50%; Figure S8f). The differences in~~

540 ~~predicted versus observed PNs may be associated with assumed background, dilution, and/or~~

541 ~~temperature used to reach steady-state~~ (Schroeder et al., 2020)~~. Thus, the results from F0AM will~~

542 ~~provide qualitative insight into sources and chemistry that should be investigated to better~~

543 ~~understand PN chemistry in SMA.~~

544   The classes of compounds producing higher PNs in F0AM are shown in Figure 5b. The

545 classes of compounds were selected from the parent VOC which was oxidized into the higher PN

546 (Table S2). Individual PNs with high contributions and/or are typically measured (PPN, PBzN,

547 and MPAN (methacryloyl peroxy nitrate)) or are a large fraction of PNs but have yet to be

548 measured in ambient conditions (PHAN) are shown without any connection to the parent VOC.

549 Further, both PHAN and PPN have numerous precursors while many of the other higher PNs

550 modeled by F0AM are generally associated with one precursor. At high NO_x mixing ratios, the

551 more reactive VOCs (aromatics, terpenes) contribute a large fraction of the higher PNs (>35% for

552 NO_x > 4 ppbv). As the air moves away from SMA (lower NO_x mixing ratios), contributions of

553 higher PNs from longer-lived compounds (e.g., alkanes) and later generation oxidation products

554 start dominating.

555   An interesting trend is observed for PPN and PHAN. Both peroxy acyl radicals for PPN

556 and PHAN ($C_2H_5C(O)O_2^{\cdot}$ and $CH_2(OH)C(O)O_2^{\cdot}$, respectively) are products from photooxidation

557 of many VOCs, including aromatics, alkanes, and methyl ethyl ketone (MEK). However, the

558 fractional contribution of PPN to higher PNs remains constant with decreasing NO_x while the

559 fractional contribution of PHAN increases with decreasing NO_x (Figure 5b). This stems from the

25

560 sources of $C_2H_5C(O)O_2$ versus $CH_2(OH)C(O)O_2$. The MCM mechanism, which is used for

561 F0AM, produces $C_2H_5C(O)O_2$ from the photooxidation from both short- and long-lived species

562 (isoprene, C8-aromatics, toluene, ethanol, MEK, propane, and C4-alkanes) while

563 $CH_2(OH)C(O)O_2$ is produced from the photooxidation of isoprene and ethene. For

564 $CH_2(OH)C(O)O_2$, the production is through minor channels in the photooxidation of isoprene

565 (~3% yield directly from isoprene and ~20% as a secondary product (Galloway et al., 2011)).

566 Ethene is relatively long-lived, with a lifetime ~7 hrs (OH = 5×10^6 molec. cm^{-3}) leading to the

567 delay in the production of PHAN. Note, PHAN formation in MCM/F0AM may be overestimated,

568 as Butkovskaya et al. (2006) found that the radical formed from the photooxidation of

569 glycolaldehyde decomposes to form formaldehyde and CO_2, potentially competing with the

570 pathway to form PHAN. Other studies also found that PNs were not observed by photooxidation

571 of glycoaldehyde (Magneron et al., 2005).

572 The results here in general indicate more speciated measurements of higher PNs are

573 needed. However, as highlighted in Figure 5, improved detection of or measurements of PBzN,

574 PHAN, and MPAN would allow for furthering our knowledge in PNs chemistry in urban

575 environments and their role in controlling O_x production.

576 A qualitative investigation of the precursors of PAN predicted by F0AM are shown in

577 Figure 5c. This provides a basis for further investigation of the sources over the SMA region for

578 PAN as (a) F0AM over-predicts PAN, as noted above, (b) ethanol is currently estimated, similar

579 to Schroeder et al. (2020), and (c) R(VOC) in F0AM is low due to missing precursors. Like the

580 higher PNs, highly reactive R(VOC) contributes a large portion of the PAN budget at high NO_x.

581 The short-lived compounds contribute ~80% of PAN over SMA at the highest NO_x mixing ratios.

582 At lower NO$_x$ mixing ratios, moving away from SMA, longer-lived compounds, such as ethanol,

583 contribute the most towards PAN production (~70%).

584   One of the interesting contributions not typically observed for PAN is MEK, which also

585 contributes to PPN and PHAN. In prior studies, MEK mixing ratios were typically 0.5 to 2.0 ppbv

586 (Bon et al., 2011; de Gouw et al., 2018; Liu et al., 2015). Over the SMA, 1.5 ppbv of MEK was

587 observed on average with values as high as 8.3 ppbv. Due to the long lifetime of MEK (~30 hrs

588 for the average photolysis rate measured and OH = 5×10^6 molec. cm^{-3}), the high mixing ratios of

589 MEK are most likely due to direct emissions (e.g., de Gouw et al., 2005; Liu et al., 2015). Thus,

590 there are potentially large sources of MEK in SMA that need to be considered in properly

591 representing PAN chemistry.

592   Another potentially important compound for PAN production is ethanol. However, this

593 compound was not measured during KORUS-AQ; instead, it was estimated based on previous

594 ground-based observations, similar to Schroeder et al. (2020). Ethanol is considered to mainly

595 come from both vehicle emissions (e.g., Millet et al., 2012) and ~~potentially~~ non-transportation

596 emissions, including cleaning agents and solvents (e.g., McDonald et al., 2018). As ethanol use is

597 predicted to increase in the future (e.g., de Gouw et al., 2012) and cleaning agents and other volatile

598 chemical products appear to scale with population (Gkatzelis et al., 2021), ethanol and MEK may

599 continue contributing towards the PAN budget in the SMA in the future.

600   As a note, two other compounds potentially important for PAN production that were not

601 measured on the DC-8 during KORUS-AQ include methylglyoxal and biacetyl (LaFranchi et al.,

602 2009). In a forested environment that was partially impacted by urban outflow, these two

603 components contributed on average 25% of the PAN budget (LaFranchi et al., 2009). In urban

604 environments, methylglyoxal is believed to mainly originate from aromatic oxidation (Ling et al.,

605 2020); whereas, biacetyl is believed to come from anthropogenic emissions (Xu et al., 2023).

606 Further, as discussed in Sect. 4.3, these two compounds may potentially be important missing HO_x

607 sources, as well. Thus, measurements of these two compounds along with ethanol is necessary to

608 better understand PAN chemistry.

609

610 **4. Observational constraints of the HO_x and O_x budget over SMA**

611 As highlighted in Figure S1, the three factors impacting instantaneous $P(O_x)$ are $R(VOC)$,

612 $P(HO_x)$, and NO_x loss processes. In Sect. 3, the NO_x loss processes were investigated and provided

613 a constraint for $R(VOC)$ to improve the investigation of $P(O_x)$. With $R(VOC)$ constrained, the

614 $RO_2^{\cdot}$ concentration can be estimated, providing a means to calculate the net $P(O_x)$ and to

615 investigate the major reactions leading to O_x loss and total HO_x ($OH + HO_2 + RO_2^{\cdot} + R(O)O_2^{\cdot}$)

616 loss. With the latter, this allows for an investigation of the major $P(HO_x)$ reactions, assuming

617 $L(HO_x)$ equals $P(HO_x)$ (see Eq. 1 – 7 in Sect. 2.3).

618

619 **4.1 Net O_x production and sources of O_x loss**

620 Using the total $R(VOC)$ from Sect. 3.3 (Figure 4a), the net $P(O_x)$ (Eq. 1 – 2) over SMA

621 during KORUS-AQ has been determined (Figure 6a). The net $P(O_x)$ peaked at 9.3~~10.3~~ ppbv hr^{-1}

622 at ~8 ppbv NO_x. If only the measured and estimated $R(VOC)$ from F0AM secondary products is

623 used to calculate net $P(O_x)$, the value decreases to 7.6~~8.8~~ ppbv hr^{-1}, but at the same NO_x mixing

624 ratio. This value is similar to values observed in other urban locations around the world (~2 – 20

625 ppbv hr^{-1}), showing that many urban areas are still impacted by high $P(O_x)$ values (Brune et al.,

626 2022; Griffith et al., 2016; Ma et al., 2022; Ren et al., 2013; Schroeder et al., 2020; Whalley et al.,

627 2016, 2018).

28

628   The NO$_x$ distribution over SMA (Figure 1) shows a large area (~127.53°E to 127.18°E, or

629   ~39 km), which corresponds to the ~~is near the~~ NO$_x$ mixing ratio that ~~with~~ results in ~~the~~ maximum

630   P(O$_x$), as shown in ~~(~~Figure 6a~~)~~. Thus, a large portion of the SMA will have high instantaneous

631   P(O$_x$) of ~~~10~~9 ppbv hr^{-1}. As the median wind speed over SMA during KORUS-AQ was ~5 m s^{-1},

632   an air parcel would remain at the highest P(O$_x$) for ~2 hrs, leading to ~18~~20~~ ppbv O$_3$ being

633   produced (not including dilution). This agrees with the ~20 ppbv increase in O$_3$ observed over the

634   Taehwa Research Forest supersite between midday and afternoon overpasses by the DC-8 during

635   KORUS-AQ (Crawford et al., 2021). Thus, though there is a substantial O$_3$ background observed

636   over SMA (Colombi et al., 2023; Crawford et al., 2021), a large contribution of the O$_3$ is due to

637   photochemical production.

638   The major reactions leading to O$_x$ loss (L(O$_x$)) are shown in Figure 6b. The two major

639   reactions that lead to O$_x$ loss are net R8 (light and dark red), or the net production of PNs (which

640   includes losses), and R11, reaction of NO$_2$ with OH (blue) (see Table 1). Note, as discussed in

641   Sect. 2.2, for the budget analysis conducted here, PAN and PPN were constrained to observations.

642   At high NO$_x$ (near emissions, ~30 ppbv), R11 (NO$_2$ + OH) dominates the L(O$_x$) budget (> 60%),

643   with net R8 (net PAN, dark red, and higher PNs, light red) contributing ~25%, and R12 – 14

644   accounting for the remaining 15% of O$_x$ loss. As NO$_x$ mixing ratios decrease (moving away from

645   emissions), the net R8 reaction, producing both PAN and higher PNs, starts contributing to larger

646   total L(O$_x$), ranging from 30 – 40%. Furthermore, the net R8 reaction contribution towards L(O$_x$)

647   remains relatively constants with NO$_x$ mixing ratios as the contribution from R11 (OH + NO$_2$)

648   decreases. At NO$_x$ mixing ratios < 3 ppbv is when non-NO$_x$ reactions (R12 – 14) contribute greater

649   than 30% of the L(O$_x$) budget. Thus, proper representation of PAN and higher PNs, both in

650   precursors and speciation, is important in properly understanding the O$_x$ budget in SMA.

29

651

4.2 HOₓ loss over the SMA

Similar to L(Oₓ), the major reactions leading to L(HOₓ) over the SMA during KORUS-AQ were the reactions of NOₓ with HOₓ, specifically NO₂ with OH (R11) and net PAN (dark red) and higher PNs (light red) production (R8) (Figure 6c). Reaction R11 is most important for NOₓ mixing ratios greater than 15 ppbv (50 – 65%). Between 5 and 15 ppbv, R11 is comparable to the net PN production (R8), where R11 comprises 35 – 50% of L(HOₓ) while net R8 (sum of higher ∑PNs and PAN) comprises 30 – 40% of L(HOₓ). At lower NOₓ mixing ratios, R11 is always smaller for L(HOₓ) than net R8, where R11 is about a factor of 2 lower than net R8. Production of ∑ANs played a minor role due to the low α_{eff}.

The self-reaction of HOₓ species (R15 – R16) contributes minimally to L(HOₓ) (less than 10%) for NOₓ mixing ratios greater than 8 ppbv. At lower NOₓ mixing ratios, R16 starts dominating L(HOₓ) budget, increasing from 8% at 8 ppbv to 50% of L(HOₓ) at NOₓ mixing ratios less than 2 ppbv. Reaction R15 remains relatively small for the L(HOₓ) budget, only reaching 7% of the L(HOₓ) budget at NOₓ mixing ratios less than 2 ppbv.

4.3 Sources of HOₓ over SMA

The analysis conducted leads to the ability to constrain HOₓ losses over the SMA during KORUS-AQ. This is important as not all typical HOₓ sources were measured on the DC-8 during the project (e.g., nitrous acid, or HONO), and HOₓ production rates directly impacts P(Oₓ) (Figure S1). Prior studies (e.g., Griffith et al., 2016; Tan et al., 2019; Whalley et al., 2018) have demonstrated that in urban environments, sources of HOₓ include photolysis of O₃ and subsequent reaction with water vapor, formaldehyde photolysis, and HONO photolysis. Furthermore, recent

674   studies have highlighted the potential importance of typically non-measured OVOCs in their

675   contribution to $P(HO_x)$ and subsequent $P(O_x)$ in an urban environment (Wang et al., 2022). To

676   constrain the $P(HO_x)$ over SMA during KORUS-AQ, the $P(HO_x)$ was assumed to be equal to the

677   observationally constrained $L(HO_x)$. Then, $P(HO_x)$ was calculated for the measurements on the

678   DC-8, including photolysis of O_3, formaldehyde, H_2O_2, and other measured OVOCs (Table 2).

679   Comparing the calculated $P(HO_x)$ and $L(HO_x)$, ~1.5 ppbv hr^{-1} $P(HO_x)$ (range 1.3 – 1.8 ppbv

680   hr^{-1}) is not accounted for, leading to ~45% of the necessary $L(HO_x)$ to maintain steady-state

681   (Figure 7). For the calculated $P(HO_x)$ budget, O_3 and formaldehyde photolysis contributed ~50%

682   and 40% of the budget, respectively, with the remainder coming from photolysis of H_2O_2 and other

683   measured OVOCs. Accounting for the unobserved $P(HO_x)$, O_3 and formaldehyde photolysis

684   contributed ~25% and ~20%, respectively.

685   Potential missing sources of $P(HO_x)$ are briefly speculated here. First, one potential source

686   is the photolysis of methylglyoxal. Using the F0AM predicted methylglyoxal, as it was not

687   measured on the DC-8, methylglyoxal would contribute ~0.24 ppbv hr^{-1} $P(HO_x)$, or ~16% of the

688   unobserved $P(HO_x)$. Another OVOC not measured on the DC-8 and expected to originate from

689   anthropogenic emissions and not from chemistry is 2,3-butanedione, or biacetyl (de Gouw et al.,

690   2018; Grosjean et al., 2002; Schauer et al., 2002; Xu et al., 2023; Zhou et al., 2020). Prior studies

691   observed 20 – 400 pptv of biacetyl (de Gouw et al., 2018; Xu et al., 2023), correspond to 0.04 –

692   0.74 ppbv hr^{-1}, or 3 – 49% of the unobserved $P(HO_x)$. Thus, between these two OVOCs, 19 – 66%

693   of the unobserved $P(HO_x)$ could be explained. Other unmeasured OVOCs could potentially

694   contribute to the observed $P(HO_x)$ (e.g., Wang et al., 2022); however, there is less constraints both

695   on the speciation and photolysis rates for these OVOCs (e.g., Mellouki et al., 2015). Finally,

696   HONO could contribute to this observed $P(HO_x)$. Up to 700 pptv of HONO was observed in SMA

697 during KORUS-AQ (Gil et al., 2021), though, this would quickly photolyze to the altitudes the

698 DC-8 flew over SMA (Tuite et al., 2021). Even at 50 – 100 pptv HONO, photolysis of HONO

699 would lead to 0.2 – 0.4 ppbv hr^{-1} P(HO$_x$), or 13 – 27% of the unobserved P(HO$_x$). Thus, between

700 methylglyoxal, biacetyl, and HONO, between 32 – 92% of the unobserved P(HO$_x$) could be

701 accounted for. This analysis highlights the importance of measuring these HO$_x$ sources to better

702 understand and constrain O$_x$ chemistry in SMA and other urban environments.

703   A comparison of HO$_x$ sources from F0AM is shown in Figure S14. As it has more complete

704 OVOCs than the observations, the contributions are different than shown in Figure 7. Both

705 observations and F0AM agree that photolysis of O$_3$ and subsequent reaction with water (R12) and

706 photolysis of formaldehyde are the two largest sources of HO$_x$. F0AM also shows that

707 methylglyoxal is an important source of HO$_x$, which is not shown in Figure 7 as methylglyoxal

708 was not measured. However, the total F0AM P(HO$_x$) was ~2.4 ppbv hr^{-1}, which was lower than

709 the observationally constrained value. This further supports either potential unmeasured OVOCs

710 coming from both emissions and chemistry and/or uncertainty in the photolysis rate constants for

711 these OVOCs (e.g., Wang et al., 2022).

712   One note about this analysis is that particulate matter collected onto the downwelling CAFS

713 optics during KORUS-AQ (see Sect. S5, Table S3, and Figure S13+). Corrections of up to 20%

714 were determined, and the associated uncertainties were also increased by 20% due to the

715 corrections. Thus, the exact amount of unmeasured P(HO$_x$) is potentially smaller than discussed.

716

717 **5. Conclusions and Implications**

718   In the Seoul Metropolitan Area (SMA), the ozone (O$_3$) mixing ratio often exceeds current

719 standards and is increasing. Many processes can impact the O$_3$ mixing ratios and exceedances.

720 Here, the processes that impact instantaneous O_3 production ($P(O_x)$, where O_x is $O_3 + NO_2$ to

721 account for possible O_3 titration) were investigated for observations collected on the NASA DC-8

722 during the 2016 NIER/NASA Korea United-States Air Quality (KORUS-AQ) study. The

723 observations indicate missing oxidized NO_x products (NO_z) that include both the short-lived

724 peroxy nitrates (ΣPNs) and alkyl and multi-functional nitrates (ΣANs). ΣPNs contributed the most

725 for the organic NO_z species. Only ~50% of the ΣPNs were speciated over SMA, which is atypical

726 as prior studies typically show closure between the speciated and total PN measurements.

727 The un-speciated ΣPNs and ΣANs were used to constrain the missing volatile organic

728 compound (VOC) reactivity (R(VOC)), as R(VOC) is important in constraining the instantaneous

729 $P(O_3)$. The missing R(VOC) was found to be 1.4 to 2.1 s^{-1}. The F0AM box model further supports

730 the role of unmeasured ΣPNs as an important temporary NO_x and radical sink over SMA. F0AM

731 predicts ~50% of the higher ΣPNs (higher ΣPNs = ΣPNs – PAN), indicating missing R(VOCs)

732 may explain the other 50%. Constraints from both the ΣPNs and ΣANs suggest that this missing

733 R(VOC) would include oxygenated VOCs (OVOCs), including aldehydes such as octanal and

734 nonanal from cooking, and alkenes from anthropogenic emissions.

735 With the constraints on the R(VOC), the net instantaneous $P(O_x)$ was determined for SMA.

736 It was found to peak at ~10 ppbv hr^{-1} at ~8 ppbv NO_x. A large fraction of the SMA area was, on

737 average, at this mixing ratio of NO_x, indicating high local $P(O_x)$. This supports the increase of ~20

738 ppbv of O_3 observed in a downwind site (Taehwa Research Forest supersite) from midday to

739 afternoon during KORUS-AQ.

740 With the comprehensive measurements on-board the DC-8, the F0AM model results, and

741 the observationally constrained R(VOC), a budget analysis on the sinks of O_3 ($L(O_x)$) and HO_x

742 ($L(HO_x)$, where $HO_x = OH + HO_2 + RO_2^{\cdot} + R(O)O_2^{\cdot}$) was performed. Due to the high R(VOC),

743 type of VOC, and the NO_2-to-NO ratio, net ΣPNs production is surprisingly a large and important

744 sink of O_x and HO_x over SMA (~25 – 40% and 15 – 40% for $L(O_x)$ and $L(HO_x)$, respectively),

745 with production of HNO_3 and radical self-reactions accounting for the other $L(O_x)$ and $L(HO_x)$

746 losses. Net ΣPNs production as an important $L(O_x)$ and $L(HO_x)$ term is significant, as ΣPNs is a

747 temporary reservoir of both NO_2 and $R(O)O_2^{\cdot}$ but has not traditionally been included in these

748 calculations. Downwind locations separated from the local NO_x and VOC emissions of the SMA

749 will experience increased $P(O_x)$ due to the release of NO_2 and $R(O)O_2^{\cdot}$. With the constraint of

750 $L(HO_x)$, $P(HO_x)$ was investigated, assuming steady-state, and unmeasured HONO plus

751 unmeasured OVOCs were found to be necessary to explain the missing HO_x sources. Both sources

752 of HO_x are either missing or highly uncertain in chemical transport models.

753   Though the high regional background and foreign sources of O_3 and its precursors elevate

754 the O_3 levels in SMA and potentially already causes the SMA to be in exceedance for O_3

755 concentrations, this study highlights the importance local, in-situ $P(O_x)$ to the SMA area, which

756 can further exacerbate the O_3 concentrations for SMA and the surrounding region. The results

757 support the observations of increasing O_3 with decreasing NO_x that has been observed for SMA in

758 prior studies. Further, the study highlights the important role of unmeasured VOCs and OVOCs

759 and the necessity to understand their sources and role in NO_x and O_3 chemistry. Further, the study

760 demonstrates the interplay of direct emissions or secondary production of PN precursors and its

761 role in net $P(O_x)$. Attempts at specifically reducing the sources of PN may adversely impact net

762 $P(O_x)$, as lower net PN chemistry may increase O_3 due to more NO_2 being available.

Data Availability

35

785 Version R6 1-min merged data used in this analysis available at
786 DOI:10.5067/Suborbital/KORUSAQ/DATA01. The F0AM setup file, input file, and output files
787 are all available at https://doi.org/10.5281/zenodo.10723227.
788

789 **Author Contribution**
790 BAN, KRT, and JHC designed the experiment and wrote the paper. BAN and KRT analyzed the
791 data. KRT ran the F0AM model and KRT and BAN analyzed the model output. BAN, DRB, PCJ,
792 RCC, JPD, GSD, SRH, LGH, JLJ, K-EK, YL, IJS, KU, and AW collected and QA/QC the data
793 during KORUS-AQ. All authors contributed to the writing and editing of the paper.

36

794 **References**

795 Archibald, A. T., Neu, J. L., Elshorbany, Y. F., Cooper, O. R., Young, P. J., Akiyoshi, H., Cox, R.

796 A., Coyle, M., Derwent, R. G., Deushi, M., Finco, A., Frost, G. J., Galbally, I. E., Gerosa, G.,

797 Granier, C., Griffiths, P. T., Hossaini, R., Hu, L., Jöckel, P., Josse, B., Lin, M. Y., Mertens, M.,

798 Morgenstern, O., Naja, M., Naik, V., Oltmans, S., Plummer, D. A., Revell, L. E., Saiz-Lopez, A.,

799 Saxena, P., Shin, Y. M., Shahid, I., Shallcross, D., Tilmes, S., Trickl, T., Wallington, T. J., Wang,

800 T., Worden, H. M., and Zeng, G.: Tropospheric ozone assessment report: A critical review of

801 changes in the tropospheric ozone burden and budget from 1850 to 2100,

802 https://doi.org/10.1525/elementa.2020.034, 2020.

803 Atkinson, R.: Kinetics of the gas-phase reactions of OH radicals with alkanes and cycloalkanes,

804 Atmos Chem Phys, 3, 2233–2307, https://doi.org/10.5194/acp-3-2233-2003, 2003.

805 Atkinson, R. and Arey, J.: Atmospheric Degradation of Volatile Organic Compounds, Chem Rev,

806 103, 4605–4638, https://doi.org/10.1021/CR0206420, 2003.

807 Atkinson, R., Baulch, D. L., Cox, R. A., Crowley, J. N., Hampson, R. F., Hynes, R. G., Jenkin, M.

808 E., Rossi, M. J., and Troe, J.: Evaluated kinetic and photochemical data for atmospheric chemistry:

809 Volume II - gas phase reactions of organic species, Atmos Chem Phys, 6, 3625–4055,

810 https://doi.org/10.5194/acp-6-3625-2006, 2006.

811 Bohn, B. and Zetzsch, C.: Kinetics and mechanism of the reaction of OH with the

812 trimethylbenzenes – experimental evidence for the formation of adduct isomers, Physical

813 Chemistry Chemical Physics, 14, 13933, https://doi.org/10.1039/c2cp42434g, 2012.

814 Bon, D. M., Ulbrich, I. M., De Gouw, J. a., Warneke, C., Kuster, W. C., Alexander, M. L., Baker,

815 a., Beyersdorf, a. J., Blake, D., Fall, R., Jimenez, J. L., Herndon, S. C., Huey, L. G., Knighton, W.

816 B., Ortega, J., Springston, S., and Vargas, O.: Measurements of volatile organic compounds at a

817 suburban ground site (T1) in Mexico City during the MILAGRO 2006 campaign: measurement

37

818 comparison, emission ratios, and source attribution, Atmos Chem Phys, 11, 2399–2421,

819 https://doi.org/10.5194/acp-11-2399-2011, 2011.

820 Bourgeois, I., Peischl, J., Neuman, J. A., Brown, S. S., Allen, H. M., Campuzano-jost, P., Coggon,

821 M. M., Digangi, J. P., Diskin, G. S., Gilman, J. B., Gkatzelis, G. I., Guo, H., Halliday, H. A.,

822 Hanisco, T. F., Holmes, C. D., Nault, B. A., Nowak, J. B., Pagonis, D., Rickly, P. S., Robinson,

823 M. A., Veres, P. R., Warneke, C., Wennberg, P. O., Washenfelder, R. A., and Wiggins, E. B.:

824 Comparison of airborne measurements of NO, NO_2, HONO, NO_y, and CO during FIREX-AQ,

825 Atmos Meas Tech, 15, 4901–4930, https://doi.org/10.5194/amt-15-4901-2022, 2022.

826 Brune, W. H., Miller, D. O., Thames, A. B., Allen, H. M., Apel, E. C., Blake, D. R., and Bui, T.

827 P.: Exploring Oxidation in the Remote Free Troposphere : Insights From Atmospheric

828 Tomography (ATom), Journal of Geophysical Research : Atmospheres, 125, c2019JD031685,

829 https://doi.org/10.1029/2019JD031685, 2019.

830 Brune, W. H., Miller, D. O., Thames, A. B., Brosius, A. L., Barletta, B., Blake, D. R., Blake, N.

831 J., Chen, G., Choi, Y., Crawford, J. H., Digangi, J. P., Diskin, G., Fried, A., Hall, S. R., Hanisco,

832 T. F., Huey, G. L., Hughes, S. C., Kim, M., Meinardi, S., Montzka, D. D., Pusede, S. E., Schroeder,

833 J. R., Teng, A., Tanner, D. J., Ullmann, K., Walega, J., Weinheimer, A., Wisthaler, A., and

834 Wennberg, P. O.: Observations of atmospheric oxidation and ozone production in South Korea,

835 Atmos Environ, 269, 118854, https://doi.org/10.1016/j.atmosenv.2021.118854, 2022.

836 Burkholder, J. B., Sander, S. P., Abbatt, J. P. D., Barker, J. R., Cappa, C. D., Crounse, J. D., Dibble,

837 T. S., Huie, R. E., Kolb, C. E., Kurylo, M. J., Orkin, V. L., Percival, C. J., Wilmouth, D. M., and

838 Wine, P. H.: Chemical Kinetics and Photochemical Data for Use in Atmospheric Studies,

839 Evaluation No. 19, Pasadena, CA, USA, 2020.

840 Butkovskaya, N. I., Pouvesle, N., Kukui, A., and Le Bras, G.: Mechanism of the OH-Initiated

841 Oxidation of Glycolaldehyde over the Temperature Range 233−296 K, J Phys Chem A, 110,

842 13492–13499, https://doi.org/10.1021/jp064993k, 2006.

843 Coggon, M. M., Stockwell, C. E., Claflin, M. S., Pfannerstill, E. Y., Lu, X., Gilman, J. B.,

844 Marcantonio, J., Cao, C., Bates, K., Gkatzelis, G. I., Lamplugh, A., Katz, E. F., Arata, C., Apel, E.

845 C., Hornbrook, R. S., Piel, F., Majluf, F., Blake, D. R., Wisthaler, A., Canagaratna, M., Lerner, B.

846 M., Goldstein, A. H., Mak, J. E., and Warneke, C.: Identifying and correcting interferences to

847 PTR-ToF- MS measurements of isoprene and other urban volatile organic compounds, Atmos

848 Meas Tech, 17, 801–825, https://doi.org/10.5194/amt-17-801-2024, 2024.

849 Cohen, A. J., Brauer, M., Burnett, R., Anderson, H. R., Frostad, J., Estep, K., Balakrishnan, K.,

850 Brunekreef, B., Dandona, L., Dandona, R., Feigin, V., Freedman, G., Hubbell, B., Jobling, A.,

851 Kan, H., Knibbs, L., Liu, Y., Martin, R., Morawska, L., Pope, C. A., Shin, H., Straif, K., Shaddick,

852 G., Thomas, M., van Dingenen, R., van Donkelaar, A., Vos, T., Murray, C. J. L., and Forouzanfar,

853 M. H.: Estimates and 25-year trends of the global burden of disease attributable to ambient air

854 pollution: an analysis of data from the Global Burden of Diseases Study 2015, The Lancet, 389,

855 1907–1918, https://doi.org/10.1016/S0140-6736(17)30505-6, 2017.

856 Colombi, N. K., Jacob, D. J., Yang, L. H., Zhai, S., Shah, V., Grange, S. K., Yantosca, R. M., Kim,

857 S., and Liao, H.: Why is ozone in South Korea and the Seoul metropolitan area so high and

858 increasing?, Atmos Chem Phys, 23, 4031–4044, https://doi.org/10.5194/acp-23-4031-2023, 2023.

859 Crawford, J. H., Ahn, J. Y., Al-Saadi, J., Chang, L., Emmons, L. K., Kim, J., Lee, G., Park, J. H.,

860 Park, R. J., Woo, J. H., Song, C. K., Hong, J. H., Hong, Y. D., Lefer, B. L., Lee, M., Lee, T., Kim,

861 S., Min, K. E., Yum, S. S., Shin, H. J., Kim, Y. W., Choi, J. S., Park, J. S., Szykman, J. J., Long,

862 R. W., Jordan, C. E., Simpson, I. J., Fried, A., Dibb, J. E., Cho, S. Y., and Kim, Y. P.: The Korea-

863   United States air quality (KORUS-AQ) field study, Elementa, 9, 1–27,

864   https://doi.org/10.1525/elementa.2020.00163, 2021.

865   Crounse, J., McKinney, K. A., Kwan, A. J., and Wennberg, P. O.: Measurement of gas-phase

866   hydroperoxides by chemical ionization mass spectrometry, Anal Chem, 78, 6726–6732,

867   https://doi.org/doi:10.1021/ac0604235, 2006.

868   Day, D. A., Wooldridge, P. J., Dillon, M. B., Thornton, J. A., and Cohen, R. C.: A thermal

869   dissociation laser-induced fluorescence instrument for in situ detection of NO_2, peroxy nitrates,

870   alkyl nitrates, and HNO_3, Journal of Geophysical Research-Atmospheres, 107, 4046,

871   https://doi.org/10.1029/2001JD000779, 2002.

872   Day, D. A., Campuzano-Jost, P., Nault, B. A., Palm, B. B., Hu, W., Guo, H., Wooldridge, P. J.,

873   Cohen, R. C., Docherty, K. S., Huffman, J. A., De Sá, S. S., Martin, S. T., and Jimenez, J. L.: A

874   systematic re-evaluation of methods for quantification of bulk particle-phase organic nitrates using

875   real-Time aerosol mass spectrometry, Atmos Meas Tech, 15, 459–483,

876   https://doi.org/10.5194/amt-15-459-2022, 2022.

877   Diskin, G. S., Podolske, J. R., Sachse, G. W., and Slate, T. A.: Open-path airborne tunable diode

878   laser hygrometer, in: Diode Lasers and Applications in Atmospheric Sensing, edited by: Fried, A.,

879   Proceedings of the Society of Photo-Optical Instrumentation Engineers (SPIE), 4817, 196–204,

880   https://doi.org/doi:10.1117/12.453736, 2002.

881   Espada, C. and Shepson, P. B.: The production of organic nitrates from atmospheric oxidation of

882   ethers and glycol ethers, Int J Chem Kinet, 37, 686–699, https://doi.org/10.1002/kin.20121, 2005.

883   Faloona, I. C., Tan, D., Lesher, R. L., Hazen, N. L., Frame, C. L., Simpas, J. B., Harder, H.,

884   Martinez, M., Di Carlo, P., Ren, X., and Brune, W. H.: A Laser-induced Fluorescence Instrument

40

885   for Detecting Tropospheric OH and HO_2 : Characteristics and Calibration, J Atmos Chem, 47,

886   139–167, https://doi.org/10.1023/B:JOCH.0000021036.53185.0e, 2004.

887   Farmer, D. K., Perring, A. E., Wooldridge, P. J., Blake, D. R., Baker, A., Meinardi, S., Huey, L.

888   G., Tanner, D., Vargas, O., and Cohen, R. C.: Impact of organic nitrates on urban ozone

889   production, Atmos Chem Phys, 11, 4085–4094, https://doi.org/10.5194/acp-11-4085-2011, 2011.

890   Fisher, J. A., Jacob, D. J., Travis, K. R., Kim, P. S., Marais, E. A., Miller, C. C., Yu, K., Zhu, L.,

891   Yantosca, R. M., Sulprizio, M. P., Mao, J., Wennberg, P. O., Crounse, J. D., Teng, A. P., Nguyen,

892   T. B., Clair, J. M. S., Cohen, R. C., Romer, P., Nault, B. A., Wooldridge, P. J., Jimenez, J. L.,

893   Campuzano-Jost, P., Day, D. A., Hu, W., Shepson, P. B., Xiong, F., Blake, D. R., Goldstein, A.

894   H., Misztal, P. K., Hanisco, T. F., Wolfe, G. M., Ryerson, T. B., Wisthaler, A., and Mikoviny, T.:

895   Organic nitrate chemistry and its implications for nitrogen budgets in an isoprene- and

896   monoterpene-rich atmosphere: Constraints from aircraft ($SEAC^4RS$) and ground-based (SOAS)

897   observations in the Southeast US, Atmos Chem Phys, 16, https://doi.org/10.5194/acp-16-5969-

898   2016, 2016.

899   Fried, A., Walega, J., Weibring, P., Richter, D., Simpson, I. J., Blake, D. R., Blake, N. J., Meinardi,

900   S., Barletta, B., Hughes, S. C., Crawford, J. H., Diskin, G., Barrick, J., Hair, J., Fenn, M.,

901   Wisthaler, A., Mikoviny, T., Woo, J., Park, M., Kim, J., Min, K., Jeong, S., Wennberg, P. O., Kim,

902   M. J., Crounse, J. D., Teng, A. P., Bennett, R., Yang-martin, M., Shook, M. A., Huey, G., Tanner,

903   D., Knote, C., and Kim, J.: Airborne formaldehyde and volatile organic compound measurements

904   over the Daesan petrochemical complex on Korea's northwest coast during the Korea-United

905   States Air Quality study : Estimation of emission fluxes and effects on air quality, Elementa:

906   Science of the Anthropocene, 8, 1, https://doi.org/10.1525/elementa.2020.121, 2020.

907 Galloway, M. M., Huisman, A. J., Yee, L. D., Chan, A. W. H., Loza, C. L., Seinfeld, J. H., and

908 Keutsch, F. N.: Yields of oxidized volatile organic compounds during the OH radical initiated

909 oxidation of isoprene, methyl vinyl ketone, and methacrolein under high-NO_x conditions, Atmos

910 Chem Phys, 11, https://doi.org/10.5194/acp-11-10779-2011, 2011.

911 Gaudel, A., Cooper, O. R., Ancellet, G., Barret, B., Boynard, A., Burrows, J. P., Clerbaux, C.,

912 Coheur, P. F., Cuesta, J., Cuevas, E., Doniki, S., Dufour, G., Ebojie, F., Foret, G., Garcia, O.,

913 Granados-Muñoz, M. J., Hannigan, J. W., Hase, F., Hassler, B., Huang, G., Hurtmans, D., Jaffe,

914 D., Jones, N., Kalabokas, P., Kerridge, B., Kulawik, S., Latter, B., Leblanc, T., Le Flochmoën, E.,

915 Lin, W., Liu, J., Liu, X., Mahieu, E., McClure-Begley, A., Neu, J. L., Osman, M., Palm, M.,

916 Petetin, H., Petropavlovskikh, I., Querel, R., Rahpoe, N., Rozanov, A., Schultz, M. G., Schwab,

917 J., Siddans, R., Smale, D., Steinbacher, M., Tanimoto, H., Tarasick, D. W., Thouret, V.,

918 Thompson, A. M., Trickl, T., Weatherhead, E., Wespes, C., Worden, H. M., Vigouroux, C., Xu,

919 X., Zeng, G., and Ziemke, J.: Tropospheric Ozone Assessment Report: Present-day distribution

920 and trends of tropospheric ozone relevant to climate and global atmospheric chemistry model

921 evaluation, Elementa, 6, https://doi.org/10.1525/elementa.291, 2018.

922 Gil, J., Kim, J., Lee, M., Lee, G., Ahn, J., Soo, D., Jung, J., Cho, S., Whitehill, A., Szykman, J.,

923 and Lee, J.: Characteristics of HONO and its impact on O_3 formation in the Seoul Metropolitan

924 Area during the Korea-US Air Quality study, Atmos Environ, 247, 118182,

925 https://doi.org/10.1016/j.atmosenv.2020.118182, 2021.

926 Gkatzelis, G. I., Coggon, M. M., Mcdonald, B. C., Peischl, J., Aikin, K. C., Gilman, J. B., Trainer,

927 M., and Warneke, C.: Identifying Volatile Chemical Product Tracer Compounds in U.S. Cities,

928 Enviromental Science & Technology, 55, 188–199, https://doi.org/10.1021/acs.est.0c05467, 2021.

42

929   González-Sánchez, J. M., Brun, N., Wu, J., Ravier, S., and Clément, J.: On the importance of

930   multiphase photolysis of organic nitrates on their global atmospheric removal, Atmos Chem Phys,

931   23, 5851–5866, https://doi.org/10.5194/acp-23-5851-2023, 2023.

932   de Gouw, J. A., Middlebrook, A. M., Warneke, C., Goldan, P. D., Kuster, W. C., Roberts, J. M.,

933   Fehsenfeld, F. C., Worsnop, D. R., Canagaratna, M. R., Pszenny, A. A. P., Keene, W. C.,

934   Marchewka, M. L., Bertman, S. B., and Bates, T. S.: Budget of organic carbon in a polluted

935   atmosphere: Results from the New England Air Quality Study in 2002, Journal of Geophysical

936   Research: Atmospheres, 110, D16305, https://doi.org/10.1029/2004JD005623, 2005.

937   de Gouw, J. A., Gilman, J. B., Borbon, A., Warneke, C., Kuster, W. C., Goldan, P. D., Holloway,

938   J. S., Peischl, J., Ryerson, T. B., Parrish, D. D., Gentner, D. R., Goldstein, A. H., and Harley, R.

939   A.: Increasing atmospheric burden of ethanol in the United States, Geophys Res Lett, 39, L15803,

940   https://doi.org/10.1029/2012GL052109, 2012.

941   de Gouw, J. A., Gilman, J. B., Kim, S.-W., Alvarez, S. L., Dusanter, S., Graus, M., Griffith, S. M.,

942   Isaacman-VanWertz, G., Kuster, W. C., Lefer, B. L., Lerner, B. M., McDonald, B. C.,

943   Rappenglück, B., Roberts, J. M., Stevens, P. S., Stutz, J., Thalman, R., Veres, P. R., Volkamer, R.,

944   Warneke, C., Washenfelder, R. A., and Young, C. J.: Chemistry of Volatile Organic Compounds

945   in the Los Angeles Basin: Formation of Oxygenated Compounds and Determination of Emission

946   Ratios, Journal of Geophysical Research: Atmospheres, 123, 2298–2319,

947   https://doi.org/10.1002/2017JD027976, 2018.

948   Griffith, S. M., Hansen, R. F., Dusanter, S., Michoud, V., Gilman, J. B., Kuster, W. C., Veres, P.

949   R., Graus, M., de Gouw, J. A., Roberts, J., Young, C., Washenfelder, R., Brown, S. S., Thalman,

950   R., Waxman, E., Volkamer, R., Tsai, C., Stutz, J., Flynn, J. H., Grossberg, N., Lefer, B., Alvarez,

951   S. L., Rappenglueck, B., Mielke, L. H., Osthoff, H. D., and Stevens, P. S.: Measurements of

hydroxyl and hydroperoxy radicals during CalNex-LA: Model comparisons and radical budgets, Journal of Geophysical Research: Atmospheres, 121, 4211–4232, https://doi.org/10.1002/2015JD024358, 2016.

Grosjean, D., Grosjean, E., and Gertler, A. W.: On-Road Emissions of Carbonyls from Light-Duty and Heavy-Duty Vehicles, Enviromental Science & Technology, 35, 45–53, https://doi.org/10.1021/es001326a, 2002.

Hansen, R. F., Griffith, S. M., Dusanter, S., Gilman, J. B., Graus, M., Kuster, W. C., Veres, P. R., de Gouw, J. A., Warneke, C., Washenfelder, R. A., Young, C. J., Brown, S. S., Alvarez, S. L., Flynn, J. H., Grossberg, N. E., Lefer, B., Rappenglueck, B., and Stevens, P. S.: Measurements of Total OH Reactivity During CalNex-LA, Journal of Geophysical Research: Atmospheres, 126, e2020JD032988, https://doi.org/10.1029/2020JD032988, 2021.

Hurst Bowman, J., Barket, D. J., and Shepson, P. B.: Atmospheric chemistry of nonanal, Enviromental Science & Technology, 37, 2218–2225, 2003.

Jenkin, M. E., Young, J. C., and Rickard, A. R.: The MCM v3.3.1 degradation scheme for isoprene, Atmos Chem Phys, 15, 11433–11459, https://doi.org/10.5194/acp-15-11433-2015, 2015.

Jo, D. S., Emmons, L. K., Callaghan, P., Tilmes, S., and Woo, J.: Comparison of Urban Air Quality Simulations During the KORUS-AQ Campaign With Regionally Refined Versus Global Uniform Grids in the Multi-Scale Infrastructure for Chemistry and Aerosols (MUSICA) Version 0, J Adv Model Earth Syst, 15, e2022MS003458, https://doi.org/10.1029/2022MS003458, 2023.

Jordan, C. E., Crawford, J. H., Beyersdorf, A. J., Eck, T. F., Halliday, H. S., Nault, B. A., Chang, L. S., Park, J. S., Park, R., Lee, G., Kim, H., Ahn, J. Y., Cho, S., Shin, H. J., Lee, J. H., Jung, J., Kim, D. S., Lee, M., Lee, T., Whitehill, A., Szykman, J., Schueneman, M. K., Campuzano-Jost, P., Jimenez, J. L., DiGangi, J. P., Diskin, G. S., Anderson, B. E., Moore, R. H., Ziemba, L. D.,

Fenn, M. A., Hair, J. W., Kuehn, R. E., Holz, R. E., Chen, G., Travis, K., Shook, M., Peterson, D. A., Lamb, K. D., and Schwarz, J. P.: Investigation of factors controlling PM2.5 variability across the South Korean Peninsula during KORUS-AQ, Elementa, 8, https://doi.org/10.1525/elementa.424, 2020.

Kabir, M., Jagiella, S., and Zabel, F.: Thermal Stability of n-Acyl Peroxynitrates, Int J Chem Kinet, 46, 462–469, https://doi.org/10.1002/kin.20862, 2014.

Kenagy, H. S., Sparks, T. L., Ryerson, T. B., Blake, D. R., and Cohen, R. C.: Evidence of Nighttime Production of Organic Nitrates During SEAC[4]RS, FRAPPE, and KORUS-AQ, Geophys Res Lett, 47, e2020GL087860, https://doi.org/10.1029/2020GL087860, 2020.

Kenagy, H. S., Romer Present, P. S., Wooldridge, P. J., Nault, B. A., Campuzano-Jost, P., Day, D. A., Jimenez, J. L., Zare, A., Pye, H. O. T., Yu, J., Song, C. H., Blake, D. R., Woo, J. H., Kim, Y., and Cohen, R. C.: Contribution of Organic Nitrates to Organic Aerosol over South Korea during KORUS-AQ, Environ Sci Technol, 55, 16326–16338, https://doi.org/10.1021/acs.est.1c05521, 2021.

Kim, D., Cho, C., Jeong, S., Lee, S., Nault, B. A., Campuzano-jost, P., Day, D. A., Schroder, J. C., Jimenez, J. L., Volkamer, R., Pusede, S. E., Hall, S. R., Ullmann, K., Huey, L. G., Tanner, D. J., and Dibb, J.: Field observational constraints on the controllers in glyoxal (CHOCHO) reactive uptake to aerosol, Atmos Chem Phys, 22, 805–821, https://doi.org/10.5194/acp-22-805-2022, 2022a.

Kim, H., Zhang, Q., and Heo, J.: Influence of Intense secondary aerosol formation and long-range transport on aerosol chemistry and properties in the Seoul Metropolitan Area during spring time : Results from KORUS-AQ, Atmos. Chem. Phys., 18, 7149–7168, https://doi.org/10.51944/acp-2017-947, 2018.

45

Kim, H., Park, R. J., Kim, S., Brune, W. H., Diskin, G. S., Fried, A., Hall, S. R., Weinheimer, A. J., Wennberg, P., Wisthaler, A., Blake, D. R., and Ullmann, K.: Observed versus simulated OH reactivity during KORUS-AQ campaign : Implications for emission inventory and chemical environment in East Asia, Elementa, 10, 1–26, 2022b.

Kim, J., Lee, J., Han, J., Choi, J., Kim, D.-G., Park, J., and Lee, G.: Long-term Assessment of Ozone Nonattainment Changes in South Korea Compared to US, and EU Ozone Guidelines, Asian Journal of Atmospheric Environment, 15, 20–32, https://doi.org/10.5572/ajae.2021.098, 2021.

Kim, S., Huey, L. G., Stickel, R. E., Tanner, D. J., Crawford, J. H., Olson, J. R., Chen, G., Brune, W. H., Ren, X., Lesher, R., Wooldridge, P. J., Bertram, T. H., Perring, A., Cohen, R. C., Lefer, B. L., Shetter, R. E., Avery, M., Diskin, G., and Sokolik, I.: Measurement of HO2NO2 in the free troposphere during the Intercontinental Chemical Transport Experiment–North America 2004, Journal of Geophysical Research: Atmospheres, 112, D12S01, https://doi.org/10.1029/2006JD007676, 2007.

Kim, S., Sanchez, D., Wang, M., Seco, R., Jeong, D., Hughes, S., Barletta, B., Blake, D. R., Jung, J., Kim, D., Lee, G., Lee, M., Ahn, J., Lee, S.-D., Cho, G., Sung, M.-Y., Lee, Y.-H., Kim, D. B., Kim, Y., Woo, J.-H., Jo, D., Park, R., Park, J.-H., Hong, Y.-D., Hong, J.-H., Zhang, D. Y., Liu, J. J., Li, B. J., Davis, D. L., Bell, M. L., Fletcher, T., Haagen-Smit, A. J., Blacet, F. E., Edinger, J. G., Yum, S. S., Roberts, G., Kim, J. H., Song, K. Y., Kim, D. Y., Lim, Y. J., Armendariz, A., Son, Y. S., Kim, J. C., Kim, S., Kim, S. Y., Lee, M., Shim, H., Wolfe, G. M., Guenther, A. B., He, A., Hong, Y., Han, J., Kim, S., Lee, M., Kim, S., Choi, S., Seok, S., Kim, S., Kim, S. Y., Jiang, X. Y., Lee, M., Turnipseed, A., Guenther, A., Kim, J. C., Lee, S. J., Kim, S., Lee, K. Y., Kwak, K. H., Ryu, Y. H., Lee, S. H., Baik, J. J., Ryu, Y. H., Baik, J. J., Kwak, K. H., Kim, S., Moon, N., Bao, H., Shrestha, K. L., Kondo, A., Kaga, A., Inoue, Y., Ran, L., Zhao, C. S., Xu, W. Y., Lu, X. Q.,

46

Han, M., Lin, W. L., Yan, P., Xu, X. B., Deng, Z. Z., Ma, N., Liu, P. F., Yu, J., Liang, W. D., Chen, L. L., Geng, F., Tie, X., Guenther, A., Li, G., et al.: OH reactivity in urban and suburban regions in Seoul, South Korea – an East Asian megacity in a rapid transition, Faraday Discuss., 189, 231–251, https://doi.org/10.1039/C5FD00230C, 2016.

KORUS-AQ Science Team: KORUS-AQ Data, [Dataset], NASA Langley Research Center., https://doi.org/10.5067/Suborbital/KORUSAQ/DATA01, 2023.

LaFranchi, B. W., Wolfe, G. M., Thornton, J. a., Harrold, S. a., Browne, E. C., Min, K. E., Wooldridge, P. J., Gilman, J. B., Kuster, W. C., Goldan, P. D., DeGouw, J. a., McKay, M., Goldstein, a. H., Ren, X. R., Mao, J. Q., Cohen, R. C., de Gouw, J. a., Welsh-Bon, D., Chen, Z., and Brune, W. H.: Closing the peroxy acetyl (PA) radical budget: Observations of acyl peroxy nitrates (PAN, PPN and MPAN) during BEARPEX 2009, Abstracts of Papers of the American Chemical Society, 9, 289, https://doi.org/10.5194/acp-9-7623-2009, 2009.

Lee, Y. R., Huey, L. G., Tanner, D. J., Takeuchi, M., Qu, H., Liu, X., Ng, N. L., Crawford, J. H., Fried, A., Richter, D., Simpson, I. J., Blake, D. R., Blake, N. J., Meinardi, S., Kim, S., Diskin, G. S., Digangi, J. P., Choi, Y., Pusede, S. E., Wennberg, P. O., Kim, M. J., Crounse, J. D., Teng, A. P., Cohen, R. C., Romer, P. S., Brune, W., Wisthaler, A., Mikoviny, T., Jimenez, J. L., Campuzano-Jost, P., Nault, B. A., Weinheimer, A., Hall, S. R., and Ullmann, K.: An investigation of petrochemical emissions during KORUS-AQ: Ozone production, reactive nitrogen evolution, and aerosol production, Elementa, 10, 1–24, https://doi.org/10.1525/elementa.2022.00079, 2022.

Ling, Z., Xie, Q., Shao, M., Wang, Z., Wang, T., Guo, H., and Wang, X.: Formation and sink of glyoxal and methylglyoxal in a polluted subtropical environment: Observation-based photochemical analysis and impact evaluation, Atmos Chem Phys, 20, 11451–11467, https://doi.org/10.5194/acp-20-11451-2020, 2020.

1044 Liu, Y., Yuan, B., Li, X., Shao, M., Lu, S., Li, Y., Chang, C., Wang, Z., Hu, W., Huang, X., He,

1045 L., Zeng, L., Hu, M., and Zhu, T.: Impact of pollution controls in Beijing on atmospheric

1046 oxygenated volatile organic compounds (OVOCs) during the 2008 Olympic Games : observation

1047 and modeling implications, Atmos Chem Phys, 15, 3045–3062, https://doi.org/10.5194/acp-15-

1048 3045-2015, 2015.

1049 Lyu, X. P., Zeng, L. W., Guo, H., Simpson, I. J., Ling, Z. H., Wang, Y., Murray, F., Louie, P. K.

1050 K., Saunders, S. M., Lam, S. H. M., and Blake, D. R.: Evaluation of the effectiveness of air

1051 pollution control measures in Hong Kong, Environmental Pollution, 220, 87–94,

1052 https://doi.org/10.1016/j.envpol.2016.09.025, 2017.

1053 Ma, P. K., Zhao, Y., Robinson, A. L., Worton, D. R., Goldstein, A. H., Ortega, A. M., Jimenez, J.-

1054 L., Zotter, P., Prévôt, A. S. H., Szidat, S., and Hayes, P. L.: Evaluating the impact of new

1055 observational constraints on P-S/IVOC emissions, multi-generation oxidation, and chamber wall

1056 losses on SOA modeling for Los Angeles, CA, Atmos Chem Phys, 17, 9237–9259,

1057 https://doi.org/10.5194/acp-17-9237-2017, 2017.

1058 Ma, X., Tan, Z., Lu, K., Yang, X., Chen, X., Wang, H., Chen, S., Fang, X., Li, S., Li, X., Liu, J.,

1059 Liu, Y., Lou, S., Qiu, W., and Wang, H.: OH and HO 2 radical chemistry at a suburban site during

1060 the EXPLORE-YRD campaign in 2018, Atmos Chem Phys, 22, 7005–7028,

1061 https://doi.org/10.5194/acp-22-7005-2022, 2022.

1062 Magneron, I., Mellouki, A., Le Bras, G., Moortgat, G. K., Horowitz, A., and Wirtz, K.: Photolysis

1063 and OH-Initiated Oxidation of Glycolaldehyde under Atmospheric Conditions, J Phys Chem A,

1064 109, 4552–4561, https://doi.org/10.1021/jp044346y, 2005.

1065 Mao, J., Ren, X., Brune, W. H., Olson, J. R., Crawford, J. H., Fried, a., Huey, L. G., Cohen, R. C.,

1066 Heikes, B., Singh, H. B., Blake, D. R., Sachse, G. W., Diskin, G. S., Hall, S. R., and Shetter, R.

1067   E.: Airborne measurement of OH reactivity during INTEX-B, Atmos Chem Phys, 9, 163–173,

1068   https://doi.org/10.5194/acp-9-163-2009, 2009.

1069   McDonald, B. C., de Gouw, J. A., Gilman, J. B., Jathar, S. H., Akherati, A., Cappa, C. D., Jimenez,

1070   J. L., Lee-Taylor, J., Hayes, P. L., McKeen, S. A., Cui, Y. Y., Kim, S.-W., Gentner, D. R.,

1071   Isaacman-VanWertz, G., Goldstein, A. H., Harley, R. A., Frost, G. J., Roberts, J. M., Ryerson, T.

1072   B., and Trainer, M.: Volatile chemical products emerging as largest petrochemical source of urban

1073   organic emissions, Science, 359, 760–764, https://doi.org/10.1126/science.aaq0524, 2018.

1074   Mellouki, A., Wallington, T. J., and Chen, J.: Atmospheric chemistry of oxygenated volatile

1075   organic compounds: Impacts on air quality and climate, Chem Rev, 115, 3984–4014,

1076   https://doi.org/10.1021/cr500549n, 2015.

1077   Millet, D. B., Apel, E., Henze, D. K., Hill, J., Marshall, J. D., Singh, H. B., and Tessum, C. W.:

1078   Natural and Anthropogenic Ethanol Sources in North America and Potential Atmospheric Impacts

1079   of Ethanol Fuel Use, Enviromental Science & Technology, 46, 8484–8492, 2012.

1080   Min, K.-E., Washenfelder, R. a., Dubé, W. P., Langford, a. O., Edwards, P. M., Zarzana, K. J.,

1081   Stutz, J., Lu, K., Rohrer, F., Zhang, Y., and Brown, S. S.: A broadband cavity enhanced absorption

1082   spectrometer for aircraft measurements of glyoxal, methylglyoxal, nitrous acid, nitrogen dioxide,

1083   and water vapor, Atmos Meas Tech, 9, 423–440, https://doi.org/10.5194/amt-9-423-2016, 2016.

1084   Müller, M., Mikoviny, T., Feil, S., Haidacher, S., Hanel, G., Hartungen, E., Jordan, A., Märk, L.,

1085   Mutschlechner, P., Schottkowsky, R., Sulzer, P., Crawford, J. H., and Wisthaler, A.: A compact

1086   PTR-ToF-MS instrument for airborne measurements of volatile organic compounds at high

1087   spatiotemporal resolution, Atmos Meas Tech, 7, 3763–3772, https://doi.org/10.5194/amt-7-3763-

1088   2014, 2014.

1089   Nault, B. A., Campuzano-Jost, P., Day, D. A., Schroder, J. C., Anderson, B., Beyersdorf, A. J.,

1090   Blake, D. R., Brune, W. H., Choi, Y., Corr, C. A., de Gouw, J. A., Dibb, J., DiGangi, J. P., Diskin,

1091   G. S., Fried, A., Huey, L. G., Kim, M. J., Knote, C. J., Lamb, K. D., Lee, T., Park, T., Pusede, S.

1092   E., Scheuer, E., Thornhill, K. L., Woo, J.-H., and Jimenez, J. L.: Secondary organic aerosol

1093   production from local emissions dominates the organic aerosol budget over Seoul, South Korea,

1094   during KORUS-AQ, Atmos Chem Phys, 18, 17769–17800, https://doi.org/10.5194/acp-18-17769-

1095   2018, 2018.

1096   Nihill, K. J., Ye, Q., Majluf, F., Krechmer, J. E., Canagaratna, M. R., and Kroll, J. H.: Influence

1097   of the NO/NO_2 Ratio on Oxidation Product Distributions under High-NO Conditions, Environ Sci

1098   Technol, 55, 6594–6601, https://doi.org/10.1021/acs.est.0c07621, 2021.

1099   Orlando, J. J. and Tyndall, G. S.: Laboratory studies of organic peroxy radical chemistry: an

1100   overview with emphasis on recent issues of atmospheric significance, Chem Soc Rev, 41, 6294–

1101   6317, https://doi.org/10.1039/c2cs35166h, 2012.

1102   Park, R. J., Oak, Y. J., Emmons, L. K., Kim, C. H., Pfister, G. G., Carmichael, G. R., Saide, P. E.,

1103   Cho, S. Y., Kim, S., Woo, J. H., Crawford, J. H., Gaubert, B., Lee, H. J., Park, S. Y., Jo, Y. J.,

1104   Gao, M., Tang, B., Stanier, C. O., Shin, S. S., Park, H. Y., Bae, C., and Kim, E.: Multi-model

1105   intercomparisons of air quality simulations for the KORUS-AQ campaign, Elementa, 9, 1–29,

1106   https://doi.org/10.1525/elementa.2021.00139, 2021.

1107   Perring, A. E., Bertram, T. H., Farmer, D. K., Wooldridge, P. J., Dibb, J., Blake, N. J., Blake, D.

1108   R., Singh, H. B., Fuelberg, H., Diskin, G., Sachse, G., and Cohen, R. C.: The production and

1109   persistence of $\Sigma RONO_2$ in the Mexico City plume, Atmos Chem Phys, 10, 7215–7229,

1110   https://doi.org/10.5194/acp-10-7215-2010, 2010.

Perring, A. E., Pusede, S. E., and Cohen, R. C.: An observational perspective on the atmospheric impacts of alkyl and multifunctional nitrates on ozone and secondary organic aerosol., Chem Rev, 113, 5848–70, https://doi.org/10.1021/cr300520x, 2013.

Peterson, D. A., Hyer, E. J., Han, S. O., Crawford, J. H., Park, R. J., Holz, R., Kuehn, R. E., Eloranta, E., Knote, C., Jordan, C. E., and Lefer, B. L.: Meteorology influencing springtime air quality, pollution transport, and visibility in Korea, Elementa, 7, https://doi.org/10.1525/elementa.395, 2019.

Picquet-Varrault, B., Suarez-Bertoa, R., Duncianu, M., Cazaunau, M., Pangui, E., David, M., Doussin, J., Cnrs, U. M. R., Créteil, U. P., Paris, U. De, Pierre, I., and Laplace, S.: Photolysis and oxidation by OH radicals of two carbonyl nitrates : 4-nitrooxy-2-butanone and 5-nitrooxy-2-pentanone, Atmos Chem Phys, 20, 487–498, https://doi.org/10.5194/acp-20-487-2020, 2020.

Rao, H., Fullana, A., Sidhu, S., and Carbonell-barrachina, Á. A.: Emissions of volatile aldehydes from heated cooking oils, Food Chem, 120, 59–65, https://doi.org/10.1016/j.foodchem.2009.09.070, 2010.

Ren, X., Duin, D. Van, Cazorla, M., Chen, S., Mao, J., Zhang, L., Brune, W. H., Flynn, J. H., Grossberg, N., Lefer, B. L., Rappenglück, B., Wong, K. W., Tsai, C., Stutz, J., Dibb, J. E., Jobson, B. T., Luke, W. T., and Kelley, P.: Atmospheric oxidation chemistry and ozone production : Results from SHARP 2009 in Houston, Texas, Journal of Geophysical Research: Atmospheres, 118, 5770–5780, https://doi.org/10.1002/jgrd.50342, 2013.

Richter, D., Weibring, P., Walega, J. G., Fried, A., Spuler, S. M., and Taubman, M. S.: Compact highly sensitive multi-species airborne mid-IR spectrometer, Applied Physics B, 119, 119–131, https://doi.org/10.1007/s00340-015-6038-8, 2015.

1133   Rosen, R. S., Wood, E. C., Wooldridge, P. J., Thornton, J. A., Day, D. A., Kuster, W., Williams,

1134   E. J., Jobson, B. T., and Cohen, R. C.: Observations of total alkyl nitrates during Texas Air Quality

1135   Study 2000 : Implications for O_3 and alkyl nitrate photochemistry, J Geophys Res, 109, D07303,

1136   https://doi.org/10.1029/2003JD004227, 2004.

1137   Sachse, G. W., Hill, G. F., Wade, L. O., and Perry, M. G.: Fast-Response, High-Precision Carbon

1138   Monoxide Sensor using a Tunable Diode Laser Absorption Technique, Journal of Geophysical

1139   Research: Atmospheres, 92, 2071–2081, https://doi.org/doi:10.1029/JD092iD02p02071, 1987.

1140   Sai, S., Ho, H., Yu, J. Z., Chu, K. W., Yeung, L. L., Sai, S., Ho, H., Yu, J. Z., Chu, K. W., and

1141   Yeung, L. L.: Carbonyl Emissions from Commercial Cooking Sources in Hong Kong Carbonyl

1142   Emissions from Commercial Cooking Sources in Hong Kong, J Air Waste Manage Assoc, 56,

1143   1091–1098, https://doi.org/10.1080/10473289.2006.10464532, 2012.

1144   Saunders, S. M., Jenkin, M. E., Derwent, R. G., and Pilling, M. J.: Protocol for the development

1145   of the Master Chemical Mechanism, MCM v3 (Part A): tropospheric degradation of non-aromatic

1146   volatile organic compounds, Atmos Chem Phys, 3, 161–180, https://doi.org/10.5194/acp-3-161-

1147   2003, 2003.

1148   Schauer, J. J., Kleeman, M. J., Cass, G. R., and Simoneit, B. R. T.: Measurement of Emissions

1149   from Air Organic Compounds from Cooking with Seed Oils, Environ Sci Technol, 36, 567–575,

1150   https://doi.org/10.1021/es002053m, 2002.

1151   von Schneidemesser, E., McDonald, B. C., Denier van der Gon, H., Crippa, M., Guizzardi, D.,

1152   Borbon, A., Dominutti, P., Huang, G., Jansens-Maenhout, G., Li, M., Ou-Yang, C. F., Tisinai, S.,

1153   and Wang, J. L.: Comparing Urban Anthropogenic NMVOC Measurements With Representation

1154   in Emission Inventories—A Global Perspective, Journal of Geophysical Research: Atmospheres,

1155   128, https://doi.org/10.1029/2022JD037906, 2023.

1156 Schroeder, J. R., Crawford, J. H., Ahn, J. Y., Chang, L., Fried, A., Walega, J., Weinheimer, A.,

1157 Montzka, D. D., Hall, S. R., Ullmann, K., Wisthaler, A., Mikoviny, T., Chen, G., Blake, D. R.,

1158 Blake, N. J., Hughes, S. C., Meinardi, S., Diskin, G., Digangi, J. P., Choi, Y., Pusede, S. E., Huey,

1159 G. L., Tanner, D. J., Kim, M., and Wennberg, P.: Observation-based modeling of ozone chemistry

1160 in the Seoul metropolitan area during the Korea-United States Air Quality Study (KORUS-AQ),

1161 Elementa, 8, https://doi.org/10.1525/elementa.400, 2020.

1162 Seo, J., Park, D. R., Kim, J. Y., Youn, D., Lim, Y. Bin, and Kim, Y.: Effects of meteorology and

1163 emissions on urban air quality : a quantitative statistical approach to long-term records (1999 –

1164 2016) in Seoul , South Korea, Atmos Chem Phys, 18, 16121–16137, 2018.

1165 Shetter, R. E. and Müller, M.: Photolysis frequency measurements using actinic flux

1166 spectroradiometry during the PEM-Tropics mission: Instrumentation description and some results,

1167 Journal   of   Geophysical   Research-Atmospheres,   104,   5647–5661,

1168 https://doi.org/10.1029/98JD01381, 1999.

1169 Simpson, I. J., Blake, D. R., Blake, N. J., Meinardi, S., Barletta, B., Hughes, S. C., Fleming, L. T.,

1170 Crawford, J. H., Diskin, G. S., Emmons, L. K., Fried, A., Guo, H., Peterson, D. A., Wisthaler, A.,

1171 Woo, J., Barré, J., Gaubert, B., Kim, J., Kim, M. J., Kim, Y., Knote, C., Mikoviny, T., Sally, E.,

1172 Schroeder, J. R., Wang, Y., Wennberg, P. O., and Zeng, L.: Characterization , sources and

1173 reactivity of volatile organic compounds (VOCs) in Seoul and surrounding regions during

1174 KORUS-AQ,   Elementa: Science   of   the   Anthropocene,   8,   37,

1175 https://doi.org/10.1525/elementa.434, 2020.

1176 Sprengnether, M. M., Demerjian, K. L., Dransfield, T. J., Clarke, J. S., Anderson, J. G., and

1177 Donahue, N. M.: Rate Constants of Nine C6-C9 Alkanes with OH from 230 to 379 K: Chemical

1178 Tracers for [OH] , J Phys Chem A, 113, 5030–5038, https://doi.org/10.1021/jp810412m, 2009.

53

Tan, Z., Lu, K., Hofzumahaus, A., Fuchs, H., Bohn, B., Holland, F., Liu, Y., Rohrer, F., Shao, M., Sun, K., Wu, Y., Zeng, L., Zhang, Y., Zou, Q., Kiendler-Scharr, A., Wahner, A., and Zhang, Y.: Experimental budgets of OH, HO_2, and RO_2 radicals and implications for ozone formation in the Pearl River Delta in China 2014, Atmos Chem Phys, 19, 7129–7150, https://doi.org/10.5194/acp-19-7129-2019, 2019.

Teng, A. P., Crounse, J. D., Lee, L., St Clair, J. M., Cohen, R. C., and Wennberg, P. O.: Hydroxy nitrate production in the OH-initiated oxidation of alkenes, Atmos Chem Phys, 15, 4297–4316, https://doi.org/10.5194/acp-15-4297-2015, 2015.

Thornton, J. A., Wooldridge, P. J., and Cohen, R. C.: Atmospheric NO_2: In-situ laser-induced fluorescence detection at parts per trillion mixing ratios, Anal Chem, 72, 528–539, https://doi.org/doi:10.1021/ac9908905, 2000.

Travis, K. R., Crawford, J. H., Chen, G., Jordan, C. E., Nault, B. A., Kim, H., Jimenez, J. L., Campuzano-Jost, P., Dibb, J. E., Woo, J. H., Kim, Y., Zhai, S., Wang, X., McDuffie, E. E., Luo, G., Yu, F., Kim, S., Simpson, I. J., Blake, D. R., Chang, L., and Kim, M. J.: Limitations in representation of physical processes prevent successful simulation of PM2.5 during KORUS-AQ, Atmos Chem Phys, 22, 7933–7958, https://doi.org/10.5194/acp-22-7933-2022, 2022.

Tuite, K., Thomas, J. L., Veres, P. R., and Roberts, J. M.: Quantifying Nitrous Acid Formation Mechanisms Using Measured Vertical Profiles During the CalNex 2010 Campaign and 1D Column Modeling, Journal of Geophysical Research: Atmospheres, 126, e2021JD034689, https://doi.org/10.1029/2021JD034689, 2021.

Wang, W., Yuan, B., Peng, Y., Su, H., Cheng, Y., Yang, S., Wu, C., Qi, J., Bao, F., Huangfu, Y., Wang, C., Ye, C., Wang, Z., Wang, B., Wang, X., Song, W., Hu, W., Cheng, P., Zhu, M., Zheng, J., and Shao, M.: Direct observations indicate photodegradable oxygenated volatile organic

compounds (OVOCs) as larger contributors to radicals and ozone production in the atmosphere, Atmos Chem Phys, 22, 4117–4128, https://doi.org/10.5194/acp-22-4117-2022, 2022.

Wargocki, P., Weschler, J., and Williams, J.: Assessment of aldehyde contributions to PTR-MS m/z 69.07 in indoor air measurements, Environmental Science: Atmospheres, Advance Ar, https://doi.org/10.1039/d3ea00055a, 2023.

Weinheimer, A. J., Walega, J. G., Ridley, B. A., Gary, B. L., Blake, D. R., Blake, N. J., Rowland, F. S., Sachse, G. W., Anderson, B. E., and Collins, J. E.: Meridional distributions of NO_x , NO_y , and other species in the lower stratosphere and upper troposphere during AASE II, Geophys Res Lett, 21, 2583–2586, https://doi.org/10.1029/94GL01897, 1994.

Whalley, L. K., Stone, D., Bandy, B., Dunmore, R., Hamilton, J. F., Hopkins, J., Lee, J. D., Lewis, A. C., and Heard, D. E.: Atmospheric OH reactivity in central London: observations, model predictions and estimates of in situ ozone production, Atmos Chem Phys, 16, 2109–2122, https://doi.org/10.5194/acp-16-2109-2016, 2016.

Whalley, L. K., Stone, D., Dunmore, R., Hamilton, J., Hopkins, J. R., Lee, J. D., Lewis, A. C., Williams, P., Kleffmann, J., Laufs, S., and Woodward-massey, R.: Understanding in situ ozone production in the summertime through radical observations and modelling studies during the Clean air for London project (ClearfLo), Atmos Chem Phys, 18, 2547–2571, https://doi.org/10.5194/acp-18-2547-2018, 2018.

Whalley, L. K., Slater, E. J., Woodward-massey, R., Ye, C., Lee, J. D., Squires, F., Mehra, A., Worrall, S. D., Bacak, A., Bannan, T. J., Coe, H., and Percival, C. J.: Evaluating the sensitivity of radical chemistry and ozone formation to ambient VOCs and NO_x in Beijing, Atmos Chem Phys, 21, 2125–2147, https://doi.org/10.5194/acp-21-2125-2021, 2021.

1224 Wolfe, G. M., Marvin, M. R., Roberts, S. J., Travis, K. R., and Liao, J.: The Framework for 0-D

1225 Atmospheric Modeling (F0AM) v3.1, Geosci Model Dev, 9, 3309–3319,

1226 https://doi.org/10.5194/gmd-9-3309-2016, 2016.

1227 Wooldridge, P. J., Perring, A. E., Bertram, T. H., Flocke, F. M., Roberts, J. M., Singh, H. B., Huey,

1228 L. G., Thornton, J. A., Wolfe, G. M., Murphy, J. G., Fry, J. L., Rollins, A. W., LaFranchi, B. W.,

1229 and Cohen, R. C.: Total Peroxy Nitrates (ΣPNs) in the atmosphere: the Thermal Dissociation-Laser

1230 Induced Fluorescence (TD-LIF) technique and comparisons to speciated PAN measurements,

1231 Atmos Meas Tech, 3, 593–607, https://doi.org/DOI 10.5194/amt-3-593-2010, 2010.

1232 Xu, Y., Feng, X., Chen, Y., Zheng, P., Hui, L., Chen, Y., Yu, J. Z., and Wang, Z.: Development

1233 of an enhanced method for atmospheric carbonyls and characterizing their roles in photochemistry

1234 in subtropical Hong Kong, Science of The Total Environment, 896, 165135,

1235 https://doi.org/10.1016/j.scitotenv.2023.165135, 2023.

1236 Yang, G., Huo, J., Wang, L., Wang, Y., Wu, S., Yao, L., Fu, Q., and Wang, L.: Total OH Reactivity

1237 Measurements in a Suburban Site of Shanghai J, Journal of Geophysical Research: Atmospheres,

1238 127, 1–20, https://doi.org/10.1029/2021JD035981, 2022.

1239 Yeh, G. K. and Ziemann, P. J.: Alkyl nitrate formation from reactions of C8-C14 n-alkanes with

1240 OH radicals in the presence of NOx: Measured yields with essential corrections for gas-wall

1241 partitioning, Journal of Physical Chemistry A, 118, 8147–8157,

1242 https://doi.org/10.1021/jp500631v, 2014.

1243 Yeo, M. J. and Kim, Y. P.: Long-term trends of surface ozone in Korea, J Clean Prod, 294, 125352,

1244 https://doi.org/10.1016/j.jclepro.2020.125352, 2021.

1245 Yuan, B., Shao, M., de Gouw, J., Parrish, D. D., Lu, S., Wang, M., Zeng, L., Zhang, Q., Song, Y.,

1246 Zhang, J., and Hu, M.: Volatile organic compounds (VOCs) in urban air: How chemistry affects

1247 the interpretation of positive matrix factorization (PMF) analysis, Journal of Geophysical

1248 Research: Atmospheres, 117, n/a-n/a, https://doi.org/10.1029/2012JD018236, 2012.

1249 Zare, A., Romer, P. S., Nguyen, T., Keutsch, F. N., Skog, K., and Cohen, R. C.: A comprehensive

1250 organic nitrate chemistry: Insights into the lifetime of atmospheric organic nitrates, Atmos Chem

1251 Phys, 18, 15419–15436, https://doi.org/10.5194/acp-18-15419-2018, 2018.

1252 Zhao, Y., Hennigan, C. J., May, A. A., Tkacik, D. S., De Gouw, J. A., Gilman, J. B., Kuster, W.

1253 C., Borbon, A., and Robinson, A. L.: Intermediate-volatility organic compounds: A large source

1254 of   secondary   organic   aerosol,   Environ   Sci   Technol,   48,   13743–13750,

1255 https://doi.org/10.1021/es5035188, 2014.

1256 Zheng, W., Flocke, F. M., Tyndall, G. S., Swanson, A., Orlando, J. J., Roberts, J. M., Huey, L. G.,

1257 and Tanner, D. J.: Characterization of a thermal decomposition chemical ionization mass

1258 spectrometer for the measurement of peroxy acyl nitrates (PANs) in the atmosphere, Atmos Chem

1259 Phys, 11, 6529–6547, https://doi.org/10.5194/acp-11-6529-2011, 2011.

1260 Zhou, Z., Tan, Q., Deng, Y., Song, D., Wu, K., Zhou, X., Huang, F., Zeng, W., and Lu, C.:

1261 Compilation of emission inventory and source profile database for volatile organic compounds :

1262 A   case   study   for   Sichuan,   China,   Atmos   Pollut   Res,   11,   105–116,

1263 https://doi.org/10.1016/j.apr.2019.09.020, 2020.

1264
1265

Tables

1267 **Table 1.** Reactions described in text along with associated rate constants and references for those
1268 rate constants.

	Reaction	*Reaction Rate*	*Reference*
R1a	$VOC+OH \xrightarrow{O_2} RO_2^.$	Varies	Atkinson (2003); Atkinson and Arey(2003); Atkinson et al. (2006); Bohn and Zetzsch (2012); Sprengnether et al. (2009)
R1b	$VOC+h\nu \xrightarrow{O_2} RO_2^.$	Varies/Measured	Shetter & Müller (1999)
R2a	$RO_2^.+NO \rightarrow (1-\alpha) RO^. +(1-\alpha) NO_2$	$2.7\times10^{-11}\times exp(390/T)$	Burkholder et al. (2020)
R2b	$RO_2^.+NO \rightarrow \alpha RONO_2$	$2.7\times10^{-11}\times exp(390/T)$	Burkholder et al. (2020)
R3	$NO_2+h\nu \rightarrow NO+O(^3P)$	Measured on DC-8	Shetter & Müller (1999)
R4	$O(^3P)+ O_2 \rightarrow O_3$	$3.2\times10^{-11}\times exp(67/T)$	Saunders et al. (2003)
R5	$RO^.+O_2 \rightarrow R(O)+HO_2$	Assumed Instantaneous	
R6	$HO_2+NO \rightarrow OH+NO_2$	$3.45\times10^{-12}\times exp(270/T)$	Saunders et al. (2003)
R7	$RCHO+OH \xrightarrow{O_2} R(O)O_2^.$	Varies	Atkinson (2003); Atkinson and Arey (2003); Atkinson et al. (2006)
R8[a]	$R(O)O_2^.+NO_2 \leftrightarrow R(O)O_2NO_2$	F: 8.69×10^{-12} cm^3 molec.$^{-1}$ s^{-1} R: 4.30×10^{-4} s^{-1}	Burkholder et al. (2020)
R9	$R(O)O_2+NO \rightarrow RO_2^.+NO_2$	$8.1\times10^{-12}\times exp(270/T)$	Burkholder et al. (2020)
R10	$O_3 + NO \rightarrow O_2 + NO_2$	$2.07\times10^{-12}\times(-1400/T)$	Burkholder et al. (2020)
R11[b]	$OH+ NO_2 \rightarrow HNO_3$	1.24×10^{-11} cm^3 molec.$^{-1}$ s^{-1}	Burkholder et al. (2020)
R12	$O_3+h\nu \xrightarrow{H_2O} 2O(^1D)$	hv measured on DC-8; 2.14×10^{-10} cm^3 molec.$^{-1}$ s^{-1}	Shetter & Müller (1999); Saunders et al. (2003)
R13	$O_3+OH \rightarrow HO_2+ O_2$	$1.7\times10^{-12}\times exp(-940/T)$	Saunders et al. (2003)
R14	$O_3+ HO_2 \rightarrow OH + 2O_2$	$1.0\times10^{-14}\times exp(-490/T)$	Burkholder et al. (2020)
R15[b]	$HO_2+HO_2 \xrightarrow{H_2O} H_2O_2$	5.06×10^{-12} cm^3 molec.$^{-1}$ s^{-1}	Saunders et al. (2003)
R16	$HO_2+RO_2 \rightarrow Products$	$2.91\times10^{-13}\times exp(1300/T)$	Saunders et al. (2003)
R17	$HO_2+OH \rightarrow Products$	$4.80\times10^{-11}\times exp(250/T)$	Burkholder et al. (2020)

R18[b]	OH+NO $\rightarrow$ HONO	7.40×10^{-12} cm^3 molec.$^{-1}$ s^{-1}	Burkholder et al. (2020)
R19	HO$_2$+R(O)O$_2$ $\rightarrow$ Products	$4.30 \times 10^{-13} \times \exp(1040/T)$	Burkholder et al. (2020)

1269 [a]Only showing forward (F) and reverse (R) rate constant at 298 K and 1013 hPa and being a
1270 termolecular reaction.
1271 [b]Termolecular reaction; only showing rate at 298 K and 1013 hPa

1272 **Table 2.** List of instruments, compounds measured, accuracy/precision, and associated references
1273 used in this study.

Instrument	Species	References
University of California, Irvine, Whole Air Sampler (WAS)	Ethane, Ethene, Ethyne, Propane, Propene, i-Butane, n-Butane, 1-Butene, i-Butene, trans-2-Butene, cis-2-Butene i-Pentane, n-Pentane, 1,3-Butadiene, Isoprene, n-Hexane, n-Heptane, n-Octane, n-Nonane, n-Decane, 2,3-Dimethylbutane, 2-Methylpentane, 3-Methylpentane, Cyclopentane, Methylcyclopentane, Cyclohexane, Methylcyclohexane, Benzene, Toluene, m+p-Xylene, o-Xylene, Ethylbenzene, Styrene, i-Propylbenzene, n-Propylbenzene, 3-Ethyltoluene, 4-Ethyltoluene, 2-Ethyltoluene, 1,3,5-Trimethylbenzene, 1,2,4-Trimethylbenzene, 1,2,3-Trimethylbenzene, α-Pinene, β-Pinene, Methyl nitrate, Ethyl nitrate, i-Propyl nitrate, n-Propyl nitrate, 2-Butyl nitrate, 3-Pentyl nitrate, 2-Pentyl nitrate, 3-Methyl-2-Butyl nitrate	Simpson et al. (2020)
The Pennsylvania State University Airborne Tropospheric Hydrogen Oxides Sensor (ATHOS)	OH, HO$_2$, OH Reactivity	Faloona et al. (2004), Mao et al. (2009), Brune et al. (2019)
University of California, Berkeley, Thermal Dissociation-Laser Induced Fluorescence (TD-LIF)	NO$_2$, ΣPNs, ΣANs	Thornton et al. (2000), Day et al. (2002), Wooldridge et al. (2010)
NASA Langley Diode Laser Hygrometer (DLH)	H$_2$O	Diskin et al. (2002)
NASA Langley Diode Laser Spectrometer Measurements (DACOM)	CO, CH$_4$	Sachse et al. (1987)
University of Colorado, Boulder, Compact Atmospheric Multi-species Spectrometer (CAMS)	CH$_2$O, C$_2$H$_6$	Richter et al. (2015), Fried et al. (2020)
Gwangju Institute of Science and Technology Korean Airborne Cavity Enhances Spectrometer (K-ACES)	CHOCHO	Min et al. (2016), D. Kim et al. (2022)

60

NCAR CCD Actinic Flux Spectroradiometers (CAFS)	j-values	Shetter & Müller (1999)
Georgia Institute of Technology Chemical Ionization Mass Spectrometer (GT)	SO_2, PAN, PPN, APAN, PBzN	Kim et al. (2007), Lee et al. (2022)
University of Colorado, Boulder, High-Resolution Time-of-Flight Aerosol Mass Spectrometer	pNO_3	Nault et al. (2018), Day et al. (2022)
NCAR 4-Channel Chemiluminescence Instrument (NCAR)	NO, NO_2, O_3, NO_y	Weinheimer et al. (1994)
California Institute of Technology Chemical Ionization Mass Spectrometer (CIT)	Butene Hydroxynitrates, Butadiene Hydroxnitrates, Ethene Hydroxynitrates, Ethanal Nitrate, Isoprene Hydroxynitrates, Propene Hydroxynitrates, Propanal Nitrate, CH_3OOH, Peroxyacetic Acid, HNO_3, Hydroxyacetone, H_2O_2	Crounse et al. (2006), Teng et al. (2015)
University of Oslo Proton Transfer Reaction Time-of-Flight Mass Spectrometer (PTR-MS)	Methanol, Acetaldehyde, Acetone+Propanal, Isoprene, MVK+MACR+ISOPOOH, Benzene, Toluene, C8-alkylbenzenes, Monoterpenes, MEK	Müller et al. (2014)
NSRC Meteorological and Geographical Data	Latitude, Longitude, Altitude, Temperature, Pressure	Crawford et al. (2021)

1274
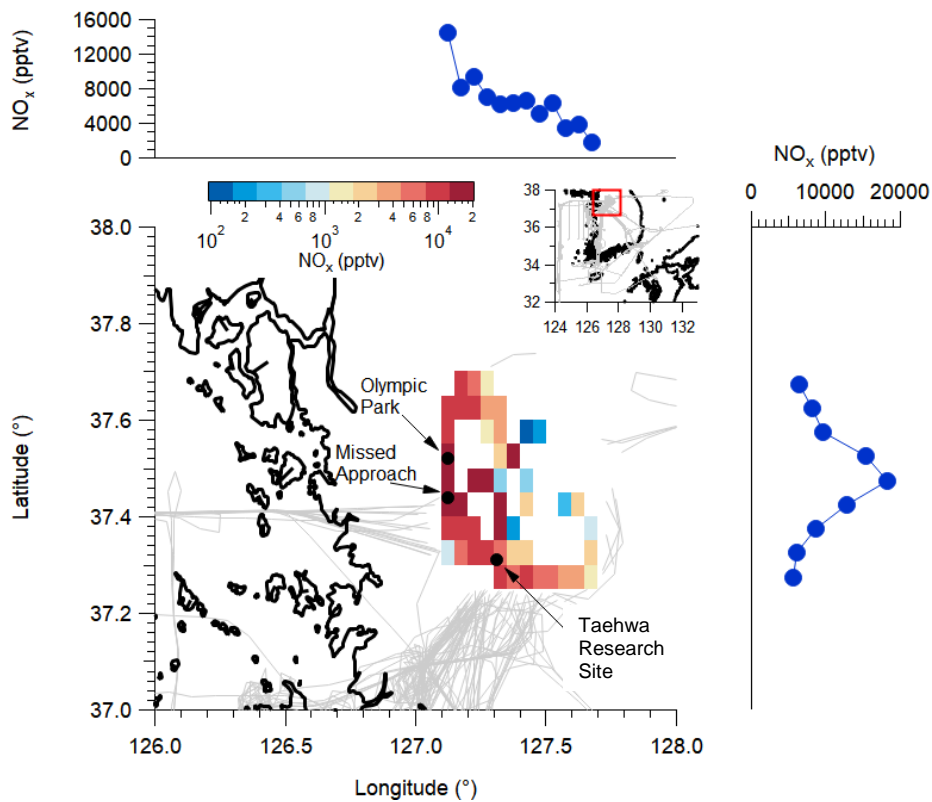
Figures

Figure 1. Binned NO$_x$ mixing ratios observed on the NASA DC-8 during the KORUS-AQ campaign. Note, the color bar scale is logarithmic. The binning is along the flight paths of the NASA DC-8 for any observations collected below 2.0 km and after 11:00 local time. The rest of the NASA DC-8 flight paths not included in the analysis are shown in grey. Three key areas from KORUS-AQ are highlighted—the Olympic Park ground site, the airfield where the NASA DC-8 conducted routine missed approaches, and the Taehwa Research ground site. The histograms above and to the left are the distribution of NO$_x$ mixing ratios longitudinally and latitudinally, respectively.
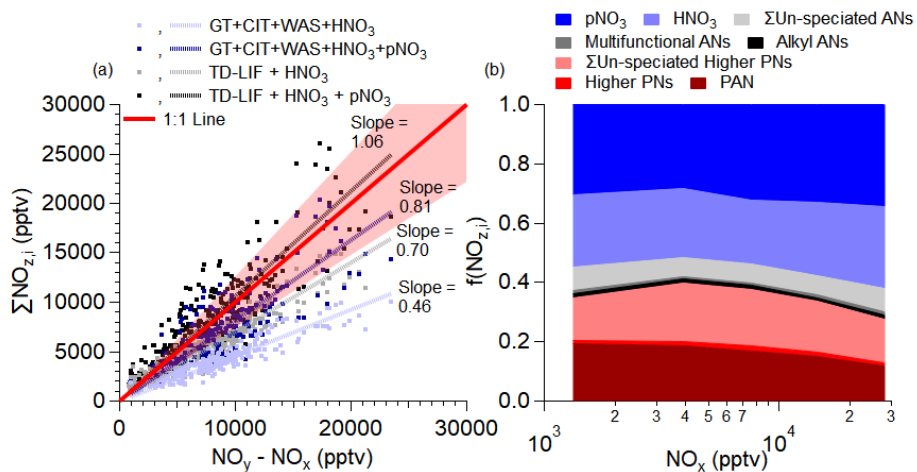
Figure 2. (a) Scatter plot of the summation of individual NO_z (NO_z is higher oxide NO_x products) measured by GT, CIT, WAS, TD-LIF, and AMS versus NO_z measured by difference between NO_y and NO_x (see Table 2 for compounds measured by each instrument). NO_x is NO measured by NCAR and NO_2 measured by LIF. The observations are for when the DC-8 was over the SMA. (b) Average contribution of measured speciated NO_z over the SMA during KORUS-AQ versus NO_x. Higher PNs is PPN + APAN + PBZN. ΣUn-speciated PNs is total peroxnitrates from TD-LIF minus total measurement from GT. Alkyl $RONO_2$ is the total small alkyl nitrate measurements from WAS. Multifunctional $RONO_2$ is the total measurements from CIT. ΣUn-speciated ANs is the total alkyl nitrates from TD-LIF minus total $RONO_2$ from CIT and WAS.
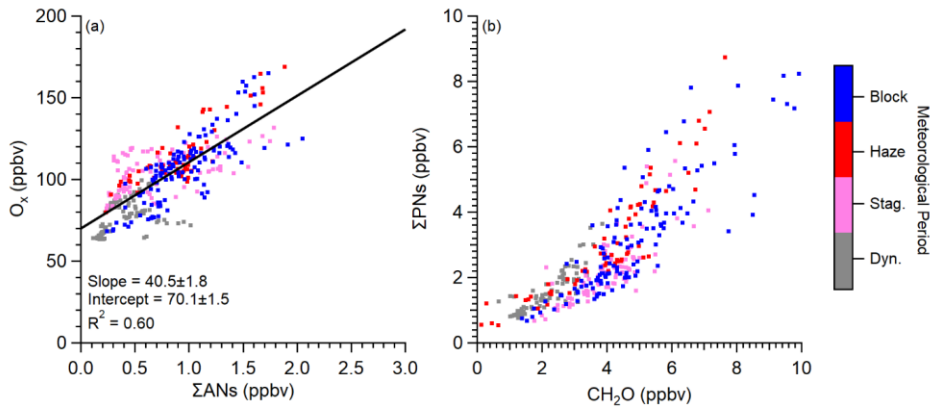
Figure 3. Scatter plot of (a) O_x versus ΣANs and (be) ΣPNs versus formaldehyde (CH_2O) over SMA (see Figure 1 for area studied). Data is colored by meteorological periods discussed in Peterson et al. (2019). Data plotted here is after 11:00 am LT to minimize impact of growing boundary layer and nocturnal residual layer mixing. The curvature in (be) is further explored in Figure S97. Eq. 8, 9, and 11 is used to convert the slope in (a) into α_{eff}. The units of the slope are ppbv ppbv^{-1}.
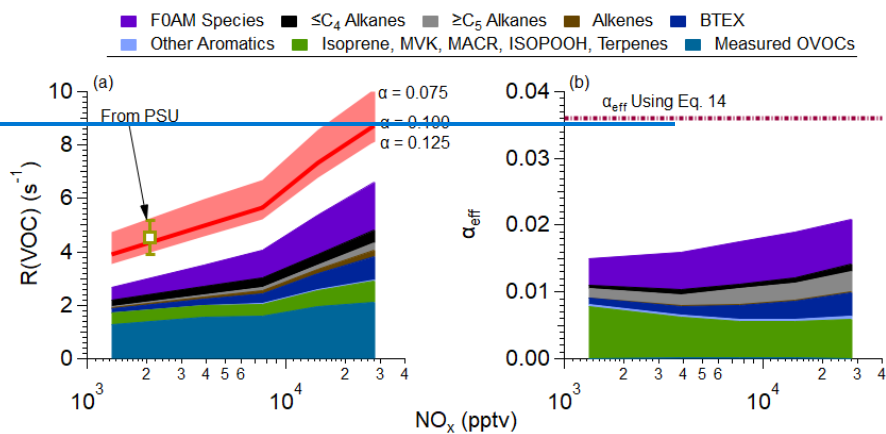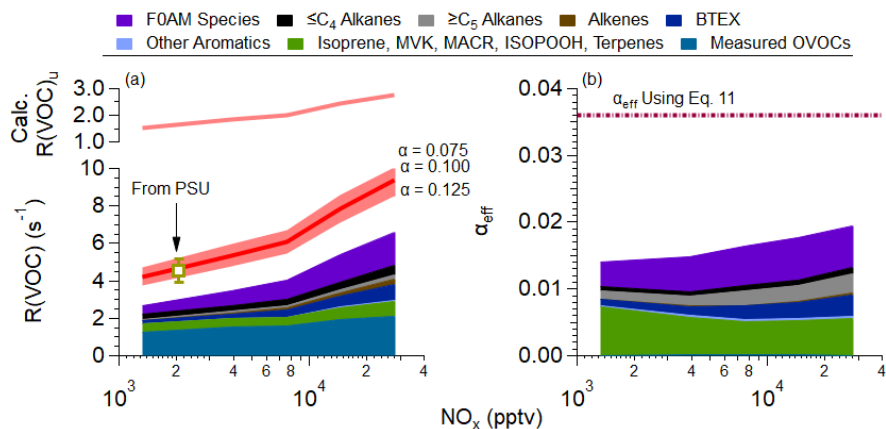
Figure 4. (a) Upper panel is the binned calculated (calc.) unmeasured VOC reactivity (R(VOC)$_u$). Note, unmeasured is for any species not measured on DC-8 or constrained by F0AM and is calculated using Eq. 13. Lower panel is bBinned VOC reactivity versus NO$_x$ observed over SMA during KORUS-AQ (see Figure 1 for the area studied). The measured observed R(VOC), labeled as "From PSU", where PSU is Pennsylvania State University, is the VOC reactivity calculated from the measured total OH reactivity with inorganic OH reactivity removed. As discussed in Brune et al. (2022), the OH reactivity has interferences at high NO$_x$ mixing ratios. The error bar is the uncertainty in the OH reactivity measurement (Brune et al., 2022). The red line represents the calculated unmeasured R(VOC), using Eq. 11, with an assumed $\alpha = 0.10$. The shaded area represents different calculated unmeasured R(VOC), assuming different α for the unmeasured R(VOC) (see Eq. 11). (b) The calculated effective α from observations versus NO$_x$. The dashed purple line is the effective α estimated from Eq. 110, using the slope from Figure 3a. For both (a)

65

1316   and (b), the colored stacked data is the calculated VOC reactivity (a) and weighted effective α (b).
1317   The values from (b) are calculated using Eq. 11. Finally, for both (a) and (b), F0AM species is the
1318   reactivity for compounds not measured on the DC-8 predicted by F0AM with an estimated α =
1319   0.05. The associated uncertainty in using different α for the F0AM predicted reactivity is explored
1320   in Figure S54.
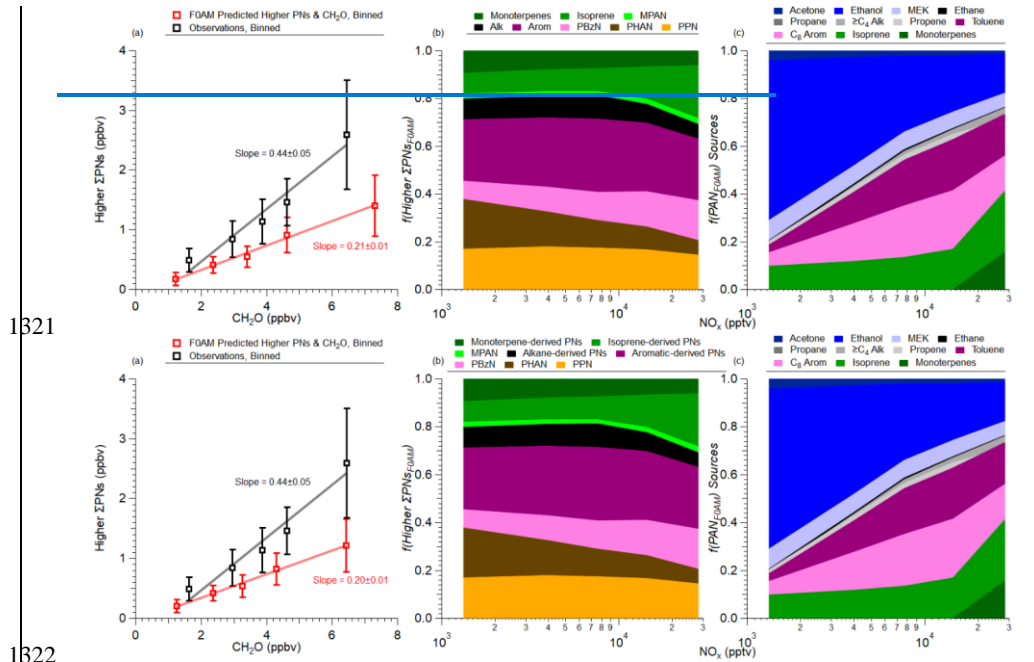
Figure 5. (a) Scatter plot of binned higher ΣPNs calculated using F0AM (red) or binned higher ΣPNs from observations (black) versus formaldehyde (CH_2O). Slopes shown are ODR fits to the binned data. PPN and PAN were constrained by observations for F0AM while all the other higher PNs were not constrained (b) Fractional contribution of the higher PNs predicted from F0AM versus NO_x. (c) Fractional contribution of different precursors to PAN, predicted by F0AM versus NO_x. For both (b) and (c), Alk is all alkanes, Arom is all aromatics, and ≥C_4 Alk is all alkanes with 4 or more carbons. See Figure S10̶8̶ for comparison of F0AM.

1330
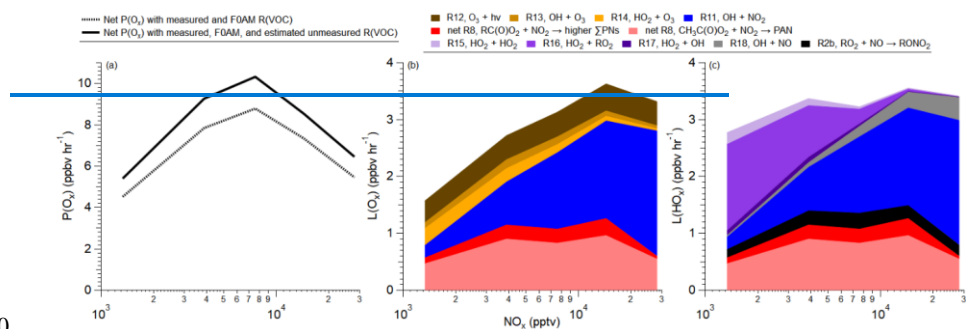
1331
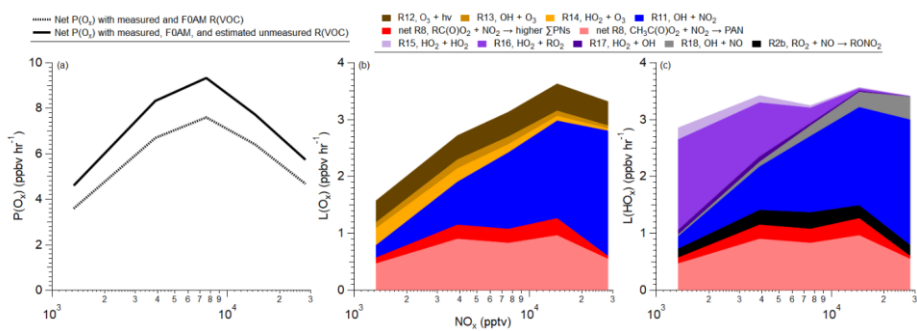
Figure 6. (a) Net O_x (O_3 + NO_2) production (see Eq. 1 and 2) predicted for SMA using measured and F0AM R(VOC) (dashed) or total R(VOC) (solid), from Figure 4a, versus NO_x. (b) Contribution of different reactions to the total O_x loss versus NO_x. (c) Contribution of different reactions to total HO_x (HO_x = OH + HO_2 + RO_2 + R(O)O_2) loss versus NO_x. The predicted RO_2 comes from the total VOC reactivity calculated in Figure 4a assuming steady-state (Eq. 7), and HO_2 the acyl peroxy radicals are from F0AM results. Note for both (b) and (c), net RC(O)O_2 + NO_2 and net $CH_3C(O)O_2$ + NO_2 are described in Eq. 3. Radical reactions contributing < 1% to the L(O_x) or L(HO_x) are not included. Also note that F0AM HO_2, $CH_3C(O)O_2$, R(O)O_2, and F0AM secondary products are used here along with observations.
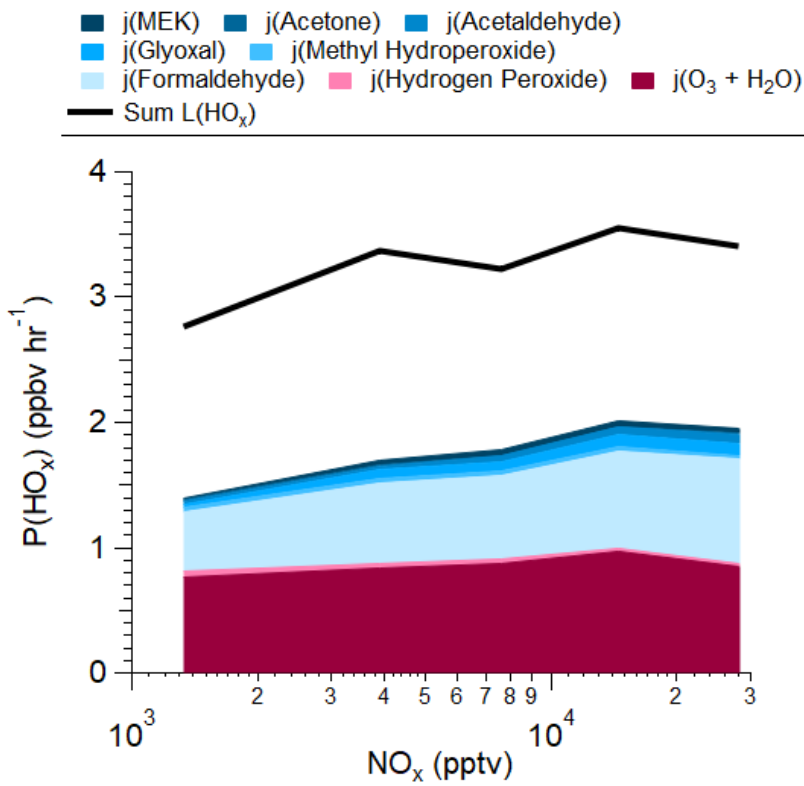
Figure 7. Calculated HO_x production from observations (colored stack) compared with the calculated HO_x loss from Figure 6c over the SMA during KORUS-AQ.